PRODUCTION OF TITANIUM DIOXIDE POWDER BY THE OXIDATION OF TITANIUM TETRACHLORIDE IN A PLASMA REACTOR

BY

MOHAMMAD TARIQUE MANGRIO

Bachelor of Engineering

Mehran University of Engg. & Technology

Jamshoro, Sind. Pakistan.

1988

Submitted to the Faculty of the
Graduate College of the
Oklahoma State University
in partial fulfillment of
the requirements for
the Degree of
MASTER OF SCIENCE
May, 1992

PRODUCTION OF TITANIUM DIOXIDE POWDER BY THE OXIDATION OF TITANIUM TETRACHLORIDE IN A PLASMA REACTOR

Thesis Approved:

Orland H. Johannes

Thesis Adviser

Marten S. High

Gary L. Foutch

Thomas C. Collins

Dean of the Graduate College

ACKNOWLEDGEMENTS

I wish to express my sincere gratitude and deep appreciation to my thesis adviser, Dr. Arland H. Johannes, for his concern, guidance, and encouragement throughout my graduate work. He is the most enthusiastic teacher I have ever had. I loved working with him.

I am grateful to my committee members, Dr. Gary L. Foutch and Dr. Martin S. High for their helpful assistance during the course of this work. Special thanks are reserved for Mr. Charles Baker, laboratory manager, for his assistance during my experimental work.

I extend my sincere thanks to Dr. Bruce Palmer of the Kerr McGee Corporation, for powder characterization on our samples.

I am indebted to my friends Nasir Junejo, Wajahat Nyaz, and Imran Shafi for their help and concern during my graduate work. I am also thankful to my father, Abdul Razzaq Mangrio for his concern, love, and support.

I am grateful to my loving brother Farooq Mangrio, without his help and love, I would not be what I am. Finally this thesis is dedicated to my loving sister, Zahra Sekandir for she has been my inspiration to achieve higher goals in life.

TABLE OF CONTENTS

LIST OF TABLES

LIST OF FIGURES

NOMENCLATURE

D_1	Inner diameter of the inner tube, cm
D_2	Outer diameter of the inner tube, cm
D_3	Inner diameter of the outer tube, cm
D_4	Outer diameter of the outer tube, cm
f	Frequency, Hz
F_r	Free energy, kcal/mol
I_p	Primary current, mA
K_a	Dielectric constant of air
K_g	Dielectric constant of glass
P	Partial pressure of monomer, torr
P_0	Equilibrium vapor pressure of monomer, torr
r^*	Critical radius
S	Supersaturation ratio
T	Temperature, °C
V	Voltage, V
V_b	Breakdown voltage, V
V_s	Secondary voltage, V
W_p	Primary power, W
Z	Zeldovich non-equilibrium correction factor
σ	Surface energy

CHAPTER I

INTRODUCTION

The production of ultrafine ceramic and metallic powders is a growing area of research for the development of high-technology ceramics, metals and cermets. Submicron powders are desired for the fabrication of materials with a low sintering temperature and a fine microstructure for reproducibility and superior chemical and mechanical properties.

In recent years, a number of standard powder production techniques have been optimized in order to meet the increasing demand for high powder quality. This implies that a process must be flexible to reach an optimum in a required particle size distribution, usually in a narrow range.

Powders are considered as populations of individual particles. Powders are typically referred to as fine (< 1.0 micron) or ultrafine (< 0.1 micron) depending on the particle size. Ultrafine powders are of interest because they offer excellent possibilities for the production of powder catalysts, ceramics, electronic devices, pigments and opacifiers, and have many other industrial applications. The uniqueness of ultrafine

powders becomes more evident as the size of the particles becomes smaller and the surface properties begin to dominate the bulk characteristics of the materials (Kuhn, 1963).

The conventional way to make fine powders is to grind a bulk material and pass it through a fine sieve. A problem with this approach is that, although the powders may be relatively fine, they may not be uniform in size. Furthermore, the very act of grinding the material may introduce metallic or other impurities (Sanders, 1984).

Preparation of ultrafine powders using nonconventional techniques have attracted increasing interest over the past years because of existing and potentially high technology applications of such powders. Johnson (1981) has categorized such nonconventional techniques as: solution techniques, vapor-phase techniques, and solid-state decomposition techniques. Most vapor-phase techniques lead to very fine unaggregated powders that in some cases are even spherical. In such techniques, the particle sizes are controlled by varying concentrations and temperature gradients during formation.

Production of ultrafine powders is among the most active areas in aerosol processing. Powders in the submicron and micron size range with a narrow particle size distribution can be produced in aerosol flow reactors. Most conventional aerosol flow reactors involve a series of complex processing, require tremendous amount of energy to produce ultrafine powders, and are limited by the materials

of construction.

Plasma chemical synthesis of powders is a viable method of producing ultrafine, ultrapure powders needed for advanced materials. Powder synthesis using plasma reactors is an expanding area of research in material processing. This technique offers the advantage of a single step continuous process, utilizing a large variety of reactants. Ceramic and metallic powders are formed by a vapor phase reaction in a high temperature gas which is generated in the plasma reactor (Vogt, 1986).

The objective of this work is to investigate the feasibility of production of ultrafine powders, using vapor phase technique, in an alternating current plasma reactor (ACPR). This reactor is also known as an alternating current corona reactor, glow discharge reactor, or alternating current silent discharge plasma reactor. The reactors used in this work were developed, as a joint venture, by the Naval Research Center and Oklahoma State University.

A plasma reactor utilizes electrical energy to create a low temperature plasma (electric discharge) in a reactor cavity. When reactants flow in the plasma, their chemical bonds are broken by absorbing the electrical energy of the plasma. Elemental atoms result, which then recombine to form the reaction products.

The use of plasma reactors for chemical synthesis has been investigated intensively in the past and is reviewed by

Tsai (Tsai, 1991). The use of plasma reactors is finding increasing applications in fields like power engineering, space travel technology, thermal processing, chemical, metallurgical and ceramic processing. Plasma synthesis offers the potential of improved chemical homogeneity, unique microstructural powder properties, excellent control over purity and stoichiometry, and elimination of tremendous amounts of energy involved in most reactions of industrial interest (Anderson, 1989).

Synthesis of ultrafine powders using plasma reactors have received much attention especially for the production of carbides and nitrides (Nicholson, 1988). Ruiqing Li et al. (1988) have reported the production of ultrafine and ultrapure silicon nitride powder of less than 100 nm, using a RF (radio frequency) plasma furnace.

The vapor-phase oxidation reaction of titanium tetrachloride used in the production of titanium dioxide (chloride process) was selected as a model reaction for this study because it is a well studied reaction and has been the subject of extensive research in the past. Titanium dioxide, can be synthesized in two different polymorphic forms, anatase and rutile. Rutile is the most desirable product because it is the most stable phase at any temperature and pressure, has superior pigmentary characteristics, high dielectric constant, and a high refractive index.

Titanium dioxide is one of the leading aerosol

generated powders produced in the United States. The United States produces more than 50% of the world's titanium dioxide, followed by West Germany (11%) and the United Kingdom (10%). The high refractive index, lack of absorption of visible light, stability at high temperatures, and nontoxicity of titanium dioxide are the reasons why it has become the predominant white pigment in the world. Titanium dioxide is also used extensively as a catalyst and has potential applications in electronics, plastics, and in the ceramics industry.

Titanium dioxide powders have been produced by two processes, the sulfate process and the chloride process. There has been a rapid growth in the chloride process since 1970, particularly in the United States, where it amounts to 75% of the total production capacity. Titanium dioxide powders obtained from the chloride process are generally a mixture of anatase and rutile forms. Study of the transformation mechanism of anatase to rutile has attracted many researchers in powder processing, several studies suggest the use of additives such as aluminum trichloride, to increase the rutile content (Criado et al. 1983, and Shannon et al. 1965).

In summary, this work presents an investigation of the feasibility for use of an alternating current plasma reactor, for the production of titanium dioxide by the vapor-phase oxidation of titanium tetrachloride, without the use of any additives.

CHAPTER II

LITERATURE REVIEW

This chapter briefly reviews some of the experimental and theoretical studies available in the literature, which are concerned with plasma and plasma processing of fine powders. The review is presented in three sections. The first section briefly discusses the gas breakdown, plasma environment and the basic types. The second section describes the importance and production of titanium dioxide in aerosol flow reactors. Finally, the third section reviews plasma synthesis of fine powders.

Gas Breakdown and Breakdown Voltage

A gas has a very low electrical conductivity resulting from relatively few free electrons and positive and negative ions. However, when an electric field is applied, electrons gain more energy than the ionization energy of the gas molecules. At this time the molecule is capable of ionizing. The new electron together with the primary one repeats the process, and an avalanche of electrons finally occurs. Such generations of rapidly succeeding avalanches can produce a space charge of slow positive ions in the gap which favors the ionization conditions for the electrons,

and produces the rapid current growth leading to "breakdown" (Tsai, 1991).

A manifestation of discharge or breakdown is emission of light, sometimes accompanied by audible noise and by current fluctuations (Loeb, 1939).

Liao and Plump (1951) concluded that the breakdown of air in a non-uniform field always occurred at a lower voltage than in a uniform field. For moderately non-uniform field electrodes such as coaxial cylinders, the breakdown voltages increase linearly with increased spacing as in a uniform field. As the spacing between electrodes becomes comparable to or greater than the diameter of either electrode, the breakdown value increased more slowly with increasing spacing. For very non-uniform field electrodes, such as a wire electrode, the breakdown characteristics were not so regular.

Liao and Plump (1951) also found that the irregular breakdown of very non-uniform fields was attributed to space charges produced by local ionization prior to breakdown in the gap. For some gases, such as nitrogen, only positive-ion space charges could be produced. For air, negative-ion space charges due to oxygen were also present which, even in a relatively small quantity, tended to complicate the breakdown in an air gap. However, for electronegative gases, which could produce a large amount of negative-ion space charges upon ionization, the breakdown characteristics were found to be very irregular.

Thornton (1939) measured the corona starting gradients in wire-cylinder gaps. He used a 50 Hz alternating voltage in his experiments. The gradients are shown in Table I for a number of gases at 760 mm Hg and 0°C.

For concentric cylindrical electrodes with two dielectric layers, the total voltage, V_b (kV), necessary to initiate the corona in the gas gap could be expressed as (Dibelius, 1964)

$$V_b = 10.96 D_2 \delta \left[\left(1 + \frac{0.308}{(\delta D)^{.5}}\right) \left(\frac{\ln(D_2/D_1)}{K_g} + \frac{\ln(D_3/D_2)}{K_a} + \frac{\ln(D_4/D_3)}{K_g} \right) \right]$$

where K_a = dielectric constant of air

K_g = dielectric constant of glass

D_1 = inner diameter of the inner tube, cm

D_2 = outer diameter of the inner tube, cm

D_3 = inner diameter of the outer tube, cm

D_4 = outer diameter of the outer tube, cm

δ = density of air, g/cc

This is the equation for the effective value of the voltage required to start visual corona.

Plasma and Plasma Chemical Processing

Plasma can be defined as a partially ionized gas consisting of molecules, atoms, ions, electrons and free radicals, each moving with a certain velocity (Thorpe, 1989). Broadly speaking, plasma can be described as a system with electrical neutrality composed of positive and

TABLE I

CORONA STARTING GRADIENTS FOR VARIOUS GASES

Gas	Corona Starting Gradient Voltage (kV/cm)
Air	35.5
H_2	15.5
He	4.0
O_2	29.1
N_2	38.0
Cl_2	85.0
CO	45.5
CO_2	26.2
NH_3	56.7
N_2O	55.3
H_2S	52.1
SO_2	67.2
CS_2	64.2
CH_4	22.3
CH_3Cl	45.6
CH_3I	75.0
CH_3Br	97.0
CH_2Cl_2	126
$CHCl_3$	162
CCl_4	204

negative charge carriers.

There are two important characteristics of plasmas that need to be considered. First, there are major differences between thermal activation and electrical activation. Thomas et al. (1941), suggested that in thermal activation, energy would be concentrated in a given bond and causes chemical reaction, whereas in electrical activation, the collision with an electron produces activation directly without adding to the translational or rotational energy of the molecules. Secondly, as Chen (1974) pointed out, the motion of particles must be controlled by electromagnetic forces instead of hydrodynamic forces.

Plasmas can be classified into three basic kinds: corona, glow, and arc discharge. The various types of plasmas are characterized by the relation of current density and ratio of pressure to electric field strength, as shown in Figure 1 (Dundas, 1969).

Corona Discharge

A corona type discharge is characterized by a low current carrying column with a voltage gradient in the order of electrical breakdown strength of the gas (Debelius,1964). Corona discharge is soft, bluish in color indicating the incomplete breakdown of a gas at, or near atmospheric pressure (Coffman, 1965). In a corona discharge at atmospheric pressure the electrons have an energy distribution from just above zero to somewhat above the

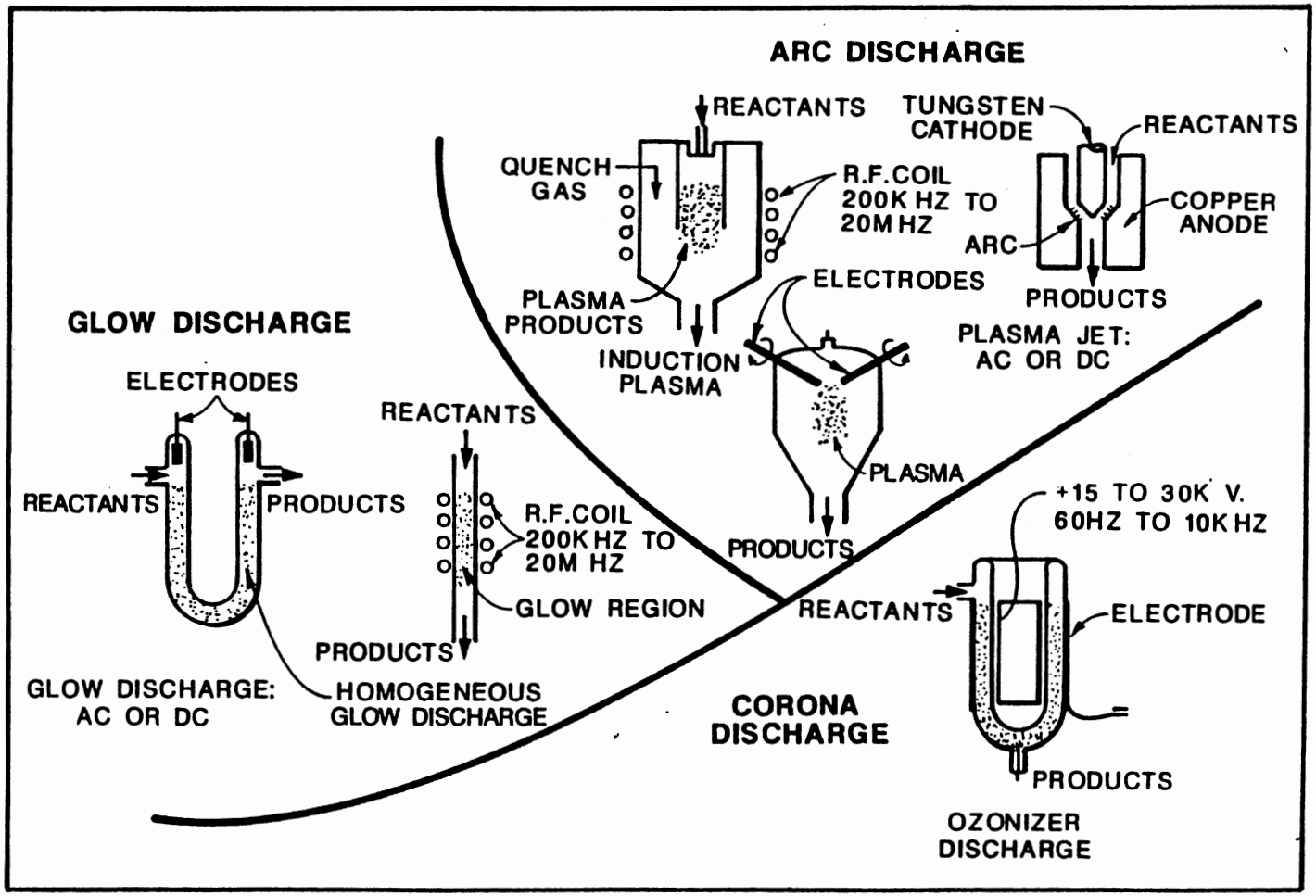

Figure 1. Plasma Operating Regions (Reference 7).

ionization potential for the gas in which the corona occurs. Since the electron energy necessary to produce excited states and free radicals is lower than that necessary to produce a positive ion and an electron, there are many more free radicals produced than positive ions.

Glow Discharge

Glow discharges are typically observed at much lower pressures (about 0.1 to 10 torr), where the electron mean free path is too long for gas collisions to be important. The electrons pick up large amounts of energy from the electric field and bombard the anode or tube wall which may then fluoresce (Kaufman, 1969). Glow discharges are non-equilibrium gas discharges and are largely or completely self-sustained. Glows are generally limited to low degrees of ionization and operate most readily at low gas density (Klyarfel'd, 1964).

When glow discharge is generated by an alternating current instead of a direct current, each electrode alternately acts as the cathode. Chapman (1980) indicated that conventional frequency was not very effective because the time during which the insulator charged up was much less than half the period of the alternating current supply. This implies that most of the time the discharge would be off.

Arc Discharge

Arc discharge, sometimes referred to as hot discharge, is characterized by exceptionally low cathode fall of potential and high current density (Loeb, 1939). This type of discharge occurs in atmospheric air as well as at lower or higher pressures and in various gases and vapors (Boenig, 1982). The arc has a high temperature and the current is carried almost entirely by mobile electrons of negligible mass. The free electron temperature is relatively close to that of the discharge gas.

Production of Titanium Dioxide

Titanium dioxide powders have been produced via two processes, i.e., the sulfate process and the chloride process. In the sulfate process, the essential step is hydrolysis under carefully controlled conditions of an acid solution of titanyl sulfate, followed by calcination of the hydrous precipitate. In the chloride process, the essential step is burning of titanium tetrachloride in oxygen to yield titanium dioxide and chlorine (Kirk and Othmer,1983). Titanium dioxide powders produced by the chloride process were first introduced commercially by Du Pont in 1958 and in Europe by British Titan Products Co.,(now the Tioxide Group) in 1965.

There has been a rapid growth in the production capacity of titanium dioxide using chloride process since

1970, particularly in the United States, where it amounts to 75% of the total titanium dioxide production capacity. The prime reasons for changeover to the chloride process from the sulfate process are that it is a continuous process, it is a more compact process, recovery and recycle of chlorine can be achieved, and a pure product with superior quality is obtained. However, there are certain disadvantages: the raw materials of high titanium content, e.g, rutile, are expensive; it is technologically an extremely difficult process; there are severe high temperature and corrosion problems; there are toxicity hazards caused by large amounts of chlorine (Kirk and Othmer, 1983). This work will only concentrate on the production of titanium dioxide via the chloride route.

Titanium dioxide is one of the major aerosol-generated products. Most of the research in the past has been devoted towards the production of titanium dioxide by the oxidation of titanium tetrachloride in conventional aerosol flow reactors. Very little work has been done in this regard using plasma reactors. However, a brief review is presented here.

Antipov et al. (1965) studied the kinetics of the closed-cycle production of titanium dioxide powders with recycling of the chlorine formed for chlorination of the original titanium ore. They calculated an activation energy of 18.3 kcal/mole for the reaction and recommended a temperature range of 1000-1100 °C for a high quality

product.

Parker (1972) summarized the results of thermodynamic equilibrium calculations on a system comprising of the elements Ti, Cl, and O in the temperature range 1327-2227 °C (the vapor phase reaction of titanium tetrachloride with oxygen). He noted that very high yields of titanium dioxide are possible in the range 90-95% of the original $TiCl_4$, in the temperature range 1427-1827 °C with ratios of Ti and O of 2.6:1. However, his data provides no information on particle size or kinetics of the reaction.

Kato et al. (1974) prepared titanium dioxide powders with 98% rutile content. This was obtained by vapor phase reaction of $TiCl_4$,H_2 and CO_2 at temperatures above 1000 °C. The average particle sizes of the products was reported in the range of 0.11 - 0.66 μm. They also stated that particle sizes decreased with increasing reaction temperatures.

Suyama et al. (1975) investigated the formation of titanium dioxide powders by vapor phase reaction of titanium tetrachloride with oxygen to elucidate the mechanism of rutile formation. They concluded that rutile formation became appreciable at effective reaction temperatures of 900-1300 °C, and increased with rising temperatures. They also showed that the ratio of rutile nucleation increased at both low and high oxygen concentrations. Rutile nucleation was not a function of titanium tetrachloride concentration. They postulated that the critical size of rutile nuclei is smaller than that of anatase nuclei. Therefore, conditions

that favor a high supersaturation of the monomer will favor anatase formation, because relatively large nuclei will be formed at high saturations. Conversely, for low supersaturation rutile will form. Table II shows a typical set of reaction conditions and rutile content for their experiments.

TABLE II

REACTION CONDITIONS AND RUTILE CONTENT

Reaction temp. °C	Total flow rate ml/min	Gas composition (vol%, balance N_2) $TiCl_4$	O_2	Rutile (wt%)
900	273	2.8	18.3	3.3
1000	273	3.0	18.3	13.5
1100	273	2.8	18.3	24.4
1300	254	3.6	19.7	36.8
1100	235	4.3	4.3	15.5
1100	308	2.7	32.5	23.7
1100	316	2.7	97.3	37.2
1100	294	0.6	34.0	21.4
1100	227	0.9	81.5	45.0

The work of Suyama et al. (1975) is the only contribution in the open literature that provides an insight into the nucleation process for titanium dioxide production from titanium tetrachloride.

Matijavic et al. (1977) described a procedure for preparation of titanium dioxide hydrosols consisting of spherical particles of narrow size distributions. Their

method involved aging of highly acidic solutions of titanium tetrachloride (containing Na_2SO_4) at elevated temperatures. They proposed a mechanism of particle formation which considered the hydrolysis of titanium ions and formation of strong titanium-sulfate complexes that slowly decompose on heating to yield hydrolyzed titanium(IV) ions, which are used up in the particle growth.

Visca et al. (1979) studied the preparation of TiO_2 powders by hydrolysis of aerosol consisting of liquid titanium(IV) compounds. Their experimental procedure consisted of generation of liquid aerosols of hydrolyzable titanium compounds which were subsequently reacted with water vapor to give titanium dioxide. They reported TiO_2 particles of a narrow size distribution with modal diameters ranging between 0.06 and 0.6 micron, when titanium(IV) ethoxide was used as a starting material. However, TiO_2 powders resulting from the hydrolysis of $TiCl_4$ aerosols, consisted of particles of a broader size distribution.

Komiyama et al. (1984) prepared ultrafine TiO_2 powders by chemical vapor deposition of titanium tetraisopropoxide. They observed that particle formation reactions were catalyzed by titanium dioxide deposits on the reactor wall, even at temperatures as low as 250 °C. The titanium dioxide particles were amorphous and porous with a specific surface area of 300 m^2/g.

Morooka et al. (1989) synthesized titanium dioxide powders by the oxidation of $TiCl_4$ in a two stage reactor, with titanium tetrachloride being fed either into only the first or both stages. Their experimental results indicated that the maximum rutile content was attained at 1000 °C. They also pointed out that fusion of titanium dioxide particles is controlled by the surface diffusion of oxygen ions.

Plasma Powder Processing

Over the past few years there has been an increasing interest in the potential of plasma processing of ultrafine powders. Plasma processing of fine powders includes topics such as production of pigments and ultrafine powders, plasma spray coating, metallurgical extraction, and synthesis of carbides, nitrides, and other inorganic materials (Waldi, 1972).

Most of the previous studies in fine powder processing have been aimed at the formation of materials with specific compositions or properties and economic assessment of such processes. A variety of plasma devices have been used for such studies, a review of which is beyond the scope of this work. The reader is referred to Waldie (1972) and Young and Pfender (1985) for more comprehensive reviews. However, a brief review focusing mainly on the production of ultrafine powders and metal oxides is presented here.

Thorpe et al. (1971) prepared zirconia (Zro_2) from zircon sand, using a plasma arc furnace. Plasma-made zirconia crystallites were extremely uniform and measured only 0.1 to 0.2 microns in diameter. A new commercial process was developed (Wilks, 1972) and operated successfully. This process is also reported to be the first commercial process based on plasma chemistry, in the United States.

Schnell et al. (1978) used a 250 kW alcohol-stablized plasma torch for the production of fumed silica. Operation of this torch is characterized by the plasma-containing vortex which is formed by the rotating stablizing alcohol. A small proportion of the recirculating alcohol is vaporized from the internal surface of the vortex and forms the plasma. Plasma fumed silica produced with this reactor consisted of white, low-density powder with relatively larger surface area.

Mahawili et al. (1979) studied the kinetics of the oxidation of titanium tetrachloride in a highly diluted system, using a rotating arc plasma jet. They designed a probe generating a corona type discharge. This type of discharge is brought about by ionization of the gas surrounding a conductor, and it occurs when the potential gradient exceeds a certain value but does not extend close enough to the other electrode to cause sparking. Their results do not fit a conventional kinetic expression based on primary reactant concentration because chlorine

generation by titanium tetrachloride dissociation turned out to be instantaneously reversible. However, their work seems to be the first attempt reported in the open literature to elucidate the kinetics of oxidation of titanium tetrachloride in a plasma reactor.

Musa et al. (1987), prepared titanium dioxide by the oxidation of titanium tetrachloride, using a 1-10 kW dc power plasmatron. A plasmatron is a continuously controlable gas discharge tube which utilizes an independently generated gas discharge plasma as a conductor between a hot cathode and an anode. They produced titanium dioxide powder having particle diameters around 0.1 micron. They also showed that size of the particles of titanium dioxide powder, was dependent on temperature of reactants.

CHAPTER III

FUNDAMENTALS OF AEROSOL FORMATION

This chapter will briefly describe the classical theory of homogeneous nucleation for aerosol growth. The nucleation and condensation growth is discussed as applied to conventional aerosol flow reactors as well as to plasma reactors.

Homogeneous Nucleation

A gas-to-liquid phase transition may occur when a vapor becomes supersaturated, with a partial pressure exceeding the equilibrium vapor pressure. The term nucleation refers to the formation of new particles from a continuous phase such as a gas phase. Homogeneous nucleation, or self nucleation, whereby clusters of the vapor itself serve as nucleation sites, is the nucleation of vapor as embryos, or condensed nuclei, in the absence of foreign nuclei. Homogeneous nucleation occurs only at high levels of supersaturation. Nucleation in the presence of a sufficient quantity of foreign substances, such as aerosol particles, charged ions, or extended surfaces is called heterogeneous nucleation (Seinfeld, 1986).

Classical nucleation theory begins by considering a system of monomers and clusters in a supersaturated system. A true equilibrium cannot exist here, as the supersaturated state is inherently unstable with respect to phase change. However, a hypothetical, pseudoequilibrium state is supposed, constrained such that no clusters are allowed to exceed a certain size. The concept of pseudoequilibrium allows thermodynamics to be brought to bear on nucleation, an essentially nonequilibrium process (Warren, 1984).

The supersaturation ratio, $S = P/P_0$, is simply the monomer partial pressure divided by the equilibrium vapor pressure of the monomer. With the supersaturation ratio known, one can estimate the critical size of the particles via the Thompson equation, given below:

$$\ln S = 2 \sigma V / r^* kT$$

where σ is the surface tension, V is the molar volume (mass over liquid phase density), r^* is the radius of the critical cluster, k is the Boltzmann constant and T is the absolute temperature (Strickland, 1967).

The rate of nucleation (J), is given by the standard classical nucleation rate expression as:

$$J = ZP_{gc} = ZB_{gc}\, n_1\, e^{-Wc}$$

where Z = Zeldovich nonequilibrium correction factor

P_{gc} = cluster growth flux in units of number/volume/time

B_{gc} = frequency of monomer addition

n_1 = monomer concentration

wc = activation energy

Condensation can be defined as the growth of existing particles(of any compositions) by the addition of the condensible vapor, which is also referred to as monomer. Condensational growth, expressed as a rate of increase in mass per particle, is proportional to particle surface area in the free molecule regime, but proportional to particle diameter in the continuum regime (Warren, 1984).

As mentioned above, aerosols can form either by homogeneous or a heterogeneous nucleation. As soon as the particles form, they grow by different growth mechanisms. Gas-to-particle conversion is the most dominant mechanism for particles in the fine size range (0.01-1.0 micron). Seinfeld, 1986 discussed the three major forms of the gas-to-particle conversion processes given below:

a) diffusion-controlled growth;

b) surface reaction-controlled growth;

c) volume reaction-controlled growth.

Seinfeld concluded that the mechanism of particle growth can be explained by the evolution of aerosol size distribution. He showed that for diffusion-controlled growth, the smallest particles grow with a rate proportional to D_p^2 (square of the particle diameter) while the larger

particles grow at a rate proportional to D_p. For the case of surface reaction-controlled growth, the large particles grow at a rate proportional to D_p^2. However, in the case of volume reaction-controlled growth, the large particle grow at a rate proportional to D_p^3. Therefore, the growth mechanism can be inferred by studying the dependence of the growth rate on the particle diameter for both the small particles (free molecule regime) and the large particles (continuum regime).

Particle Growth in a Plasma Reactor

There are three routes which are available for conversion from the gas phase to a condensed phase:

1) homogeneous nucleation;

2) condensation to an existing particle;

3) heterogeneous chemistry at a particle surface.

The homogeneous nucleation is favored by the combination of fast high temperature chemistry and rapid cooling which typically exists in a plasma reactor. Following particle inception, growth may in general occur by either of (2) or (3), as well as by coagulation (Girshick, et al., 1987).

The dominant consideration in plasma synthesis is that flow cools rapidly from a very high temperature, about 10^4 K. Thus, chemical reactions that generate the condensible vapor are fast, the saturation vapor pressure drops rapidly, and hence the supersaturation ratio mounts quickly over a

narrow temperature range until it can no longer be sustained and homogeneous nucleation occurs. Because saturation ratios are large, evaporation rates are small in comparison with condensation, and can be neglected. Particle growth also occurs through collisions or through further chemical reactions.

Girshick, et al., (1987) suggested two routes to controlling the particle size: through the reactant concentration and through the cooling rate (equivalently residence time) in the temperature region for particle growth. Thus, reactant stoichiometries, plasma compositions, or injection methods that favor higher yields are also conducive to larger particle sizes, as are flow geometries or reactor configurations that allow for longer residence times, assuming that losses to walls are suppressed.

Although random Brownian motion is often assumed to be the dominant collision mechanism for ultrafine particles, conditions in an alternating current plasma reactor could cause other factors to substantially increase collision rates. In particular, electric charging effects, London-van der Waals forces, thermophoresis, and diffusion across concentration gradients might all be suspected of playing a significant role.

CHAPTER IV

EXPERIMENTAL APPARATUS AND PROCEDURES

This chapter describes the experimental apparatus and procedures used in this work. The chapter is divided into three sections. Section one gives a description of the basic reactor design and geometry of different reactors studied. Section two describes the experimental apparatus and the discharge system. Finally, section three covers the detailed experimental procedures for transformer open-circuit, non-destructive and destructive tests.

Experimental Apparatus

A schematic of the experimental apparatus and the discharge system is shown in Figure 2. The alternating current plasma reactor is a capacitive or inductive device depending on the electrode configuration. It consists of two concentric glass tubes which form an annulus for gas flow (Figure 3). All of the reactors used were fabricated using pyrex glass except for reactor E which was made out of quartz. The pyrex glass is Corning code 7740 chemical-resistant borosilicate glass with a dielectric constant of 4.6 at 25 ^{0}C. The major differences in the several discharge reactors used in this study are the annular

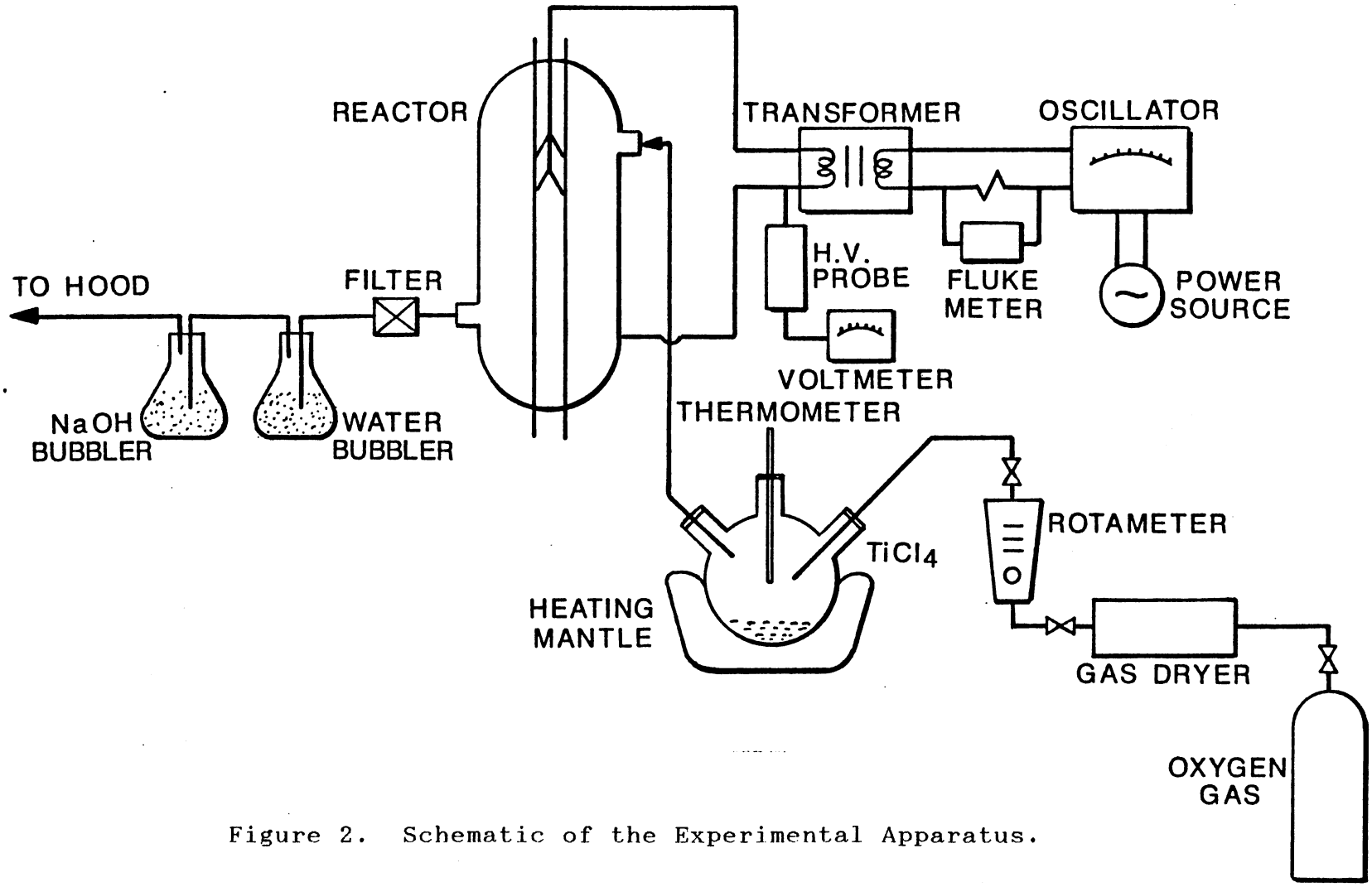

Figure 2. Schematic of the Experimental Apparatus.

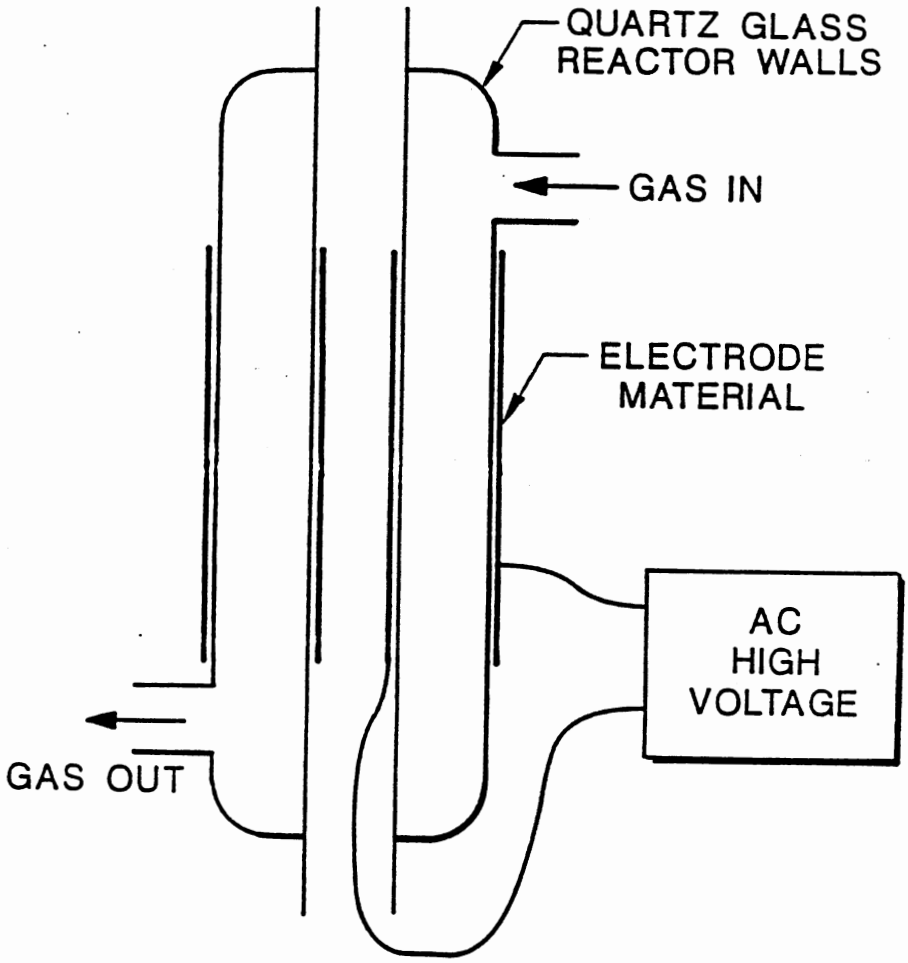

Figure 3. Discharge Reactor.

volume, effective length and the electrode configuration. These differences were used to study the effects of size of the reactor, annular gap and the residence time on the overall conversion. A summary of the discharge reactors is given in Table III. For reactors A, B, C, and D the inside of the inner tube and outside of the outer tube were coated with inorganic silver paint (Micropaint SC12 was obtained from Microcircuits Company, Inc., MI). For reactors E and F the inner electrode was silver paint while the outer electrode consisted of a molybdenum wire (1 mm diameter) tightly wrapped on the outside of outer glass tube. A wire-wrap instead of a continuous coating was used to allow visual observation of the plasma. A constant 12 wraps of wire on the reactor E and 17 wraps on the reactor F were used in all experiments. In all cases (except for the case of reactor E), contact with the electrical lead from the secondary of the transformer was provided by a 12 gauge wire which was spread apart and soldered at the tip to ensure good contact with silver paint.

Commercial grade oxygen was purchased locally from Sooner Supply Company. Oxygen gas was passed through an indicating drierite dryer to remove any moisture present in the gas. The dried gas was then passed through a calibrated Fischer rotameter (Model No. 10A6132N), which was used to adjust the flowrate of reactant gas to the desired values.

The reactant gas was then passed through a glass flask which contained titanium tetrachloride. Reagent grade

titanium tetrachloride, supplied by the Kerr McGee Corporation, was used without purification. The titanium tetrachloride was vaporized using a heating mantle. The

TABLE III

SUMMARY OF THE GEOMETRIES OF THE DISCHARGE REACTORS

Reactor	Diameter				Gap	Electrode[1] Material
	Inner Tube		Outer Tube			
	D_1 (cm)	D_2 (cm)	D_3 (cm)	D_4 (cm)	(cm)	Inner/Outer
A	1.27	1.50	2.19	2.50	0.345	SP/SP
B	1.55	1.80	2.19	2.50	0.195	SP/SP
C	1.55	1.80	2.64	3.00	0.420	SP/SP
D	1.77	2.00	2.64	3.00	0.320	SP/SP
E	1.96	1.98	2.99	3.02	0.500	CM/MW
F	0.20	0.40	1.00	1.20	0.300	CW/MW

1 SP -- silver paint
CM/ML -- copper wire/molybdenum wire

flask was heated to a constant temperature and was maintained constant so that the concentration of titanium tetrachloride entering the reactor was regulated by the amount of oxygen passed into the flask. The flask was

connected to the reactor using Teflon tubing (0.25" O.D). The temperature in the flask was measured by a thermometer. Excess oxygen was varied in all experiments but it never exceeded 2000%.

The reactant gases entered at the top port of the reactor and the products exited at the bottom port. The reaction products were passed through a filter holder containing a polycarbonate membrane filter to capture titanium dioxide particles. The chlorine gas and any unreacted titanium tetrachloride was then passed through a water bubbler to convert the unreacted titanium tetrachloride to titanium dioxide. The effluent chlorine gas was then passed through a sodium hydroxide bubbler to absorb chlorine gas. Any unabsorbed chlorine gas from NaOH bubbler was vented into the hood.

The Discharge System

The electrical system is an impedance-changing circuit. Power is supplied through a voltage transformer to one of the discharge reactors using a power amplifier (California Instruments Model 161T with a plug-in oscillator). The power amplifier is a solid state, high performance, low distortion power source, that provides a maximum of 160 VA output. The power amplifier can automatically adjust to changes in load. In a discharge system such as this, the secondary voltage of the transformer can be tuned by an oscillator. The oscillator is a Wein-bridge type and

produces a nearly perfect sine wave with less than 1% distortion from 20 to 200 Hz. The output range of the oscillator is from 40 to 5000 Hz. The iron-core transformer (Jefferson Electric Co.) is a luminous tube, high power factor transformer with a midpoint grounded secondary. The rating of the transformer is 15 kV and 60 mA for a primary voltage of 120 v at 60 Hz.

The primary current was measured by using a meter shunt of 0.5 ampere which had an equivalent voltage drop of 50 mV. A digital multimeter (Fluke Model 8050A) was used to measure the voltage difference across the shunt. The primary voltage was read off from the power amplifier panel. For the measurement of secondary voltage, a Simpson AC high voltage probe was used in conjunction with a Simpson 260 multimeter.

Transformer Open-circuit Tests

The effect of frequency on the power loss, voltage and current of the transformer can be evaluated by means of open-circuit tests. Through these tests, the operating frequency range of the system can be determined.

The experimental procedure is given as follows:

1. The secondary of the transformer was disconnected.
2. The primary voltage was set.
3. The frequency was varied from 60 Hz until the rated voltage of the transformer was reached. The electrical data were recorded.

4. Step (3) was repeated for different primary voltages.

The primary power was then calculated by multiplying the measured primary voltage and primary current.

Non-destructive Tests

As mentioned previously, a variety of discharge reactors were used for the model reaction of the oxidation of titanium tetrachloride, to study the influence of various parameters such as reactor size, residence time and the electrode arrangement. To understand the electrical characteristics of the discharge system using different reactors, non-destructive tests were performed under both unsteady and steady state conditions. Dry oxygen was used as the test gas for all the tests. For the unsteady state tests, the measurements were recorded instantaneously.

The experimental procedures for the unsteady state conditions are detailed below:

1. The power supply was turned on and the primary voltage was set. Dry oxygen was passed through the reactor at a specified flowrate.
2. Data were taken by increasing the frequency from 60 to 1000 Hz with a 100 Hz increment. When the voltage approached the breakdown voltage, the frequency was tuned smoothly until the discharge took place.
3. With the same reactor, step (2) was repeated for different primary voltages.
4. Following steps (2) and (3), the tests were continued

for another reactor.

The procedures were same for steady state tests except that after gas breakdown occurred, at least 30 minutes were allowed to pass to establish steady state conditions.

CHAPTER V

OXIDATION OF TITANIUM TETRACHLORIDE

Fine powders of titanium dioxide are produced on a large scale by processes in which volatile metal chlorides are either oxidized or hydrolyzed at high temperatures. The chemistry of these reactions is simple but serious problems are encountered in the production of fine powders because particle size must be controlled within very narrow limits. This chapter attempts to briefly review the chemistry and thermodynamics of the reaction.

Particle Formation by Vapor Phase Reaction

Fine particles form in vapor phase reactions via two processes, i.e. homogeneous nucleation and growth. The work of Suyama et al. (1975) is the only contribution in the open literature that provides insight into the nucleation process of titanium dioxide particles in aerosol flow reactors. Therefore the mechanism described by them will be considered in detail.

In the formation of titanium dioxide particles, nucleation involves the aggregation of gaseous TiO_2 molecules into a stable cluster exceeding the critical size. The formation of a cluster may be represented by:

$$TiCl_4(g) + O_2 \longrightarrow TiO_2(g) + 2Cl_2 \qquad (1)$$

$$nTiO_2(g) \longrightarrow (TiO_2)_n(s) \qquad (2)$$

A critical cluster can grow to its final size by repeated reactions on its surface, as follows:

$$TiCl_4(g) \longrightarrow TiCl_4(\text{adsorbed}) \qquad (3)$$

$$TiCl_4(\text{adsorbed}) \xrightarrow{O_2} TiO_2(s) + 2Cl_2 \qquad (4)$$

Application of the theory of homogeneous nucleation of droplets from supersaturated vapors gives the critical radius, r^*:

$$r^* = -2\,\sigma / \Delta F_r \qquad (5)$$

where σ is the surface energy of a TiO_2 particle and ΔF_r is the change in free energy per unit volume of TiO_2 formed from the vapor phase; ΔF_r is determined from the supersaturation ratio of the $TiCl_4$-O_2 system. Under equilibrium conditions, the supersaturation ratio for reaction (1) varies according to:

$$S = P_{TiO2} / P_{TiO2}^{0} = K_7 \left(P_{TiCl4}\, P_{O2} / P_{Cl2}^{2} \right) \qquad (6)$$

where K_7 is the equilibrium constant for the summary reactions:

$$TiCl_4(g) + O_2 = TiO_2(\text{anatase}) + 2Cl_2 \qquad (7a)$$

$$TiCl_4(g) + O_2 = TiO_2(\text{rutile}) + 2Cl_2 \qquad (7b)$$

The supersaturation ratio S can be expressed in terms of the partial pressure products of the reacting and equilibrium systems by:

$$S = \frac{[\ (TiCl_4).\ P(O_2)\ /\ P(Cl_2)^2\ ]_{react}}{[\ (TiCl_4).\ P(O_2)\ /\ P(Cl_2)^2\ ]_{equil}} \qquad (8)$$

For the formation of TiO_2 from the system $TiCl_4$-O_2, change in free energy is related to the saturation S by

$$\Delta F_r = -\ [\ RT\ /\ V_{TiO2}\ ]\ \ln S \qquad (9)$$

where V_{TiO2} is the molar volume of TiO_2; S, the supersaturation ratio, at a given temperature can be calculated from the amount of titanium tetrachloride converted and the initial $O_2/TiCl_4$ ratio. The surface energy of TiO_2 may be assumed to be 1000 ergs/cm^2 on the basis of the surface energy values for several oxides (Kingery, 1977).

Suyama et al. (1975) concluded that the critical size

for homogeneous nucleation of titanium dioxide is very small. Even in TiO_2 clusters of larger critical size, a few molecules can form a stable nucleus at 10% conversion of $TiCl_4$.

The particle size distribution of the product can be determined by the relative magnitudes of the nucleation rate (R_n) and growth rate (R_g). Particle size increases with increasing R_g/R_n, R_n and R_g, which are functions of the partial pressures of the reacting gases at a given temperature, and can be expressed as:

$$R_n = K_n \exp (-E_n / RT) P_{MXn}^{n} P_{O2}^{m}$$

$$R_g = K_g \exp (-E_g / RT) P_{MXn}^{p} P_{O2}^{q}$$

Accordingly, the particle size distribution varies with reaction temperature as well as gas concentration, the effects of which depends on the values of p-n and q-m. For the growth of rutile crystals from $TiCl_4$ and O_2 at 900° to 1100°C, Suyama, et al., (1975) obtained E_G = 33 kcal/mol.

Thermodynamics of the Oxidation of Titanium tetrachloride

The position of equilibrium for the vapor-phase oxidation reaction of titanium tetrachloride is favorable for the production of TiO_2, typical values of free energy changes are given in Table IV. The rate of reaction is

negligible below 600°C in a conventional aerosol flow reactor, but increases rapidly above this temperature. This suggests that equilibrium may be established in a reaction time of a millisecond at high temperature, such as in a plasma reactor. It is therefore necessary to quench the mixture to ensure completion of the reaction, ensure the provision of suitable nucleating agents to control flocculation and crystalline form, prohibit excessive growth of the pigment particles, and prevent massive growth of titanium dioxide on the reactor walls.

TABLE IV

TYPICAL VALUES OF ENERGY CHANGES

Temperature K	ΔH_f kcal/mol	ΔG kcal/mol
298	-43.4	-38.9
900	-42.6	-30.0
1200	-42.0	-25.9
2000	-40.2	-15.7

CHAPTER VI

RESULTS OF NON-DESTRUCTIVE TESTS

This chapter presents the results of open-circuit transformer tests and non-destructive tests for using a variety of discharge reactors. The details of the experimental data are given in Appendices A and B.

Open-circuit and Non-destructive Tests

The influence of frequency on the power loss, voltage and current of the transformer can be evaluated by means of open-circuit tests. Figures 4 and 5 show the effects of primary current and secondary voltage as a function of frequency under open-circuit conditions, respectively. The primary current is found to reach a minimum and then increase with increased frequency while the secondary voltage always increases as frequency increases. With an open-circuit, the primary current is very small. This indicates the effect of very high inductance and some resistance. As expected, the primary current increases more rapidly than the secondary voltage.

A series of non-destructive tests were performed at atmospheric pressure and room temperature to determine the electrical characteristics of the discharge system. The

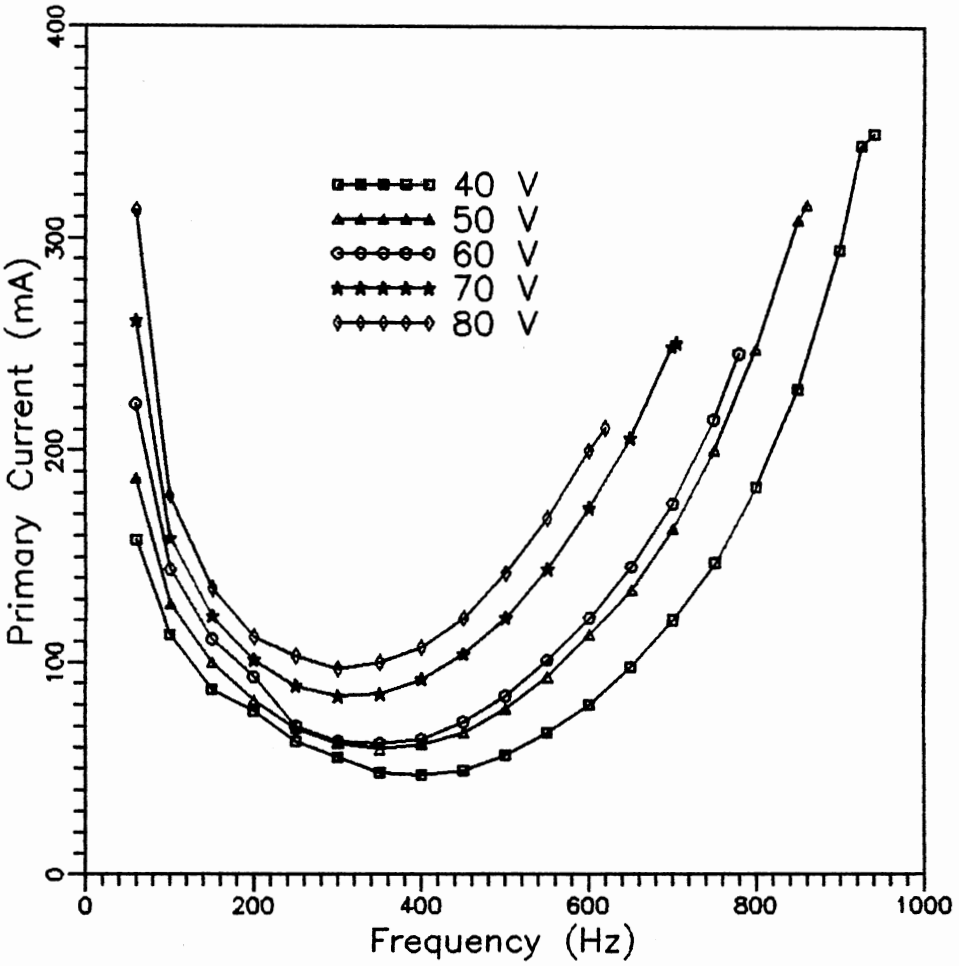

Figure 4. Effect of Frequency on Open-Circuit Primary Current for Various Primary Voltages.

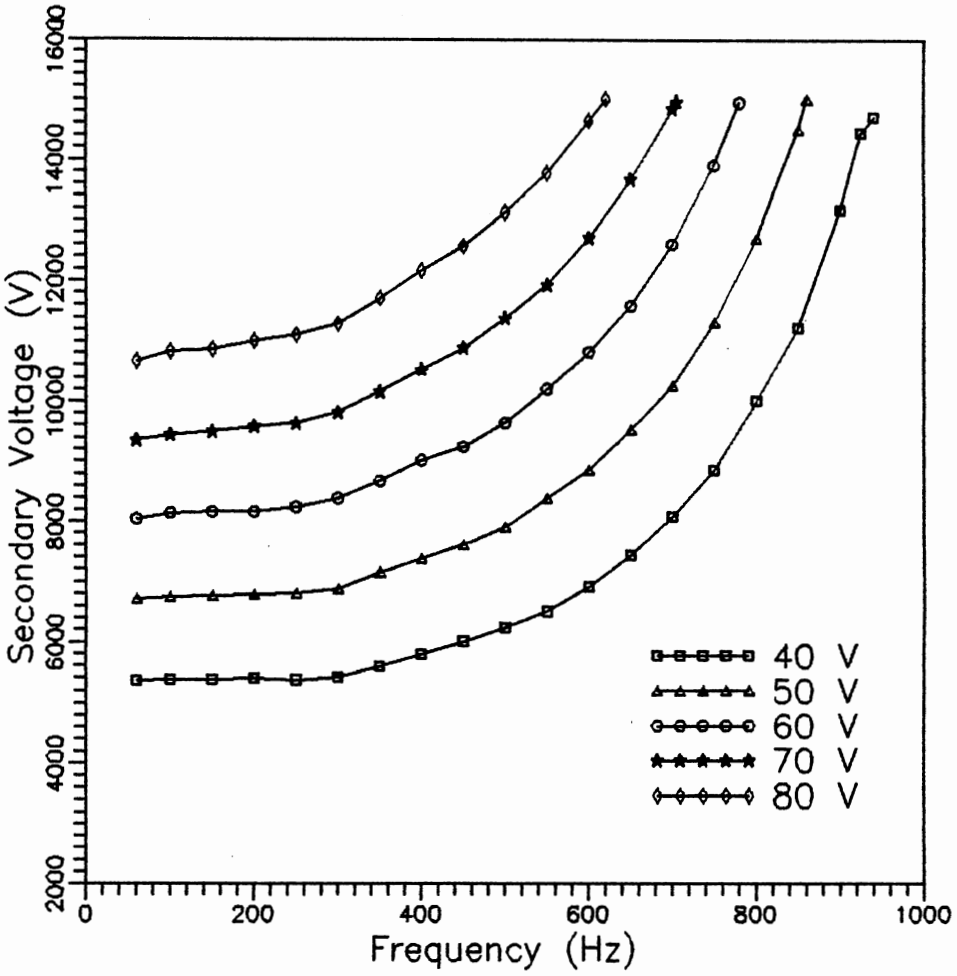

Figure 5. Effect of Frequency on Open-Circuit Secondary Voltage for Various Primary Voltages.

flowrate of oxygen gas was kept constant at 1054 ml/min in all the tests.

Before the start of a glow, a discharge reactor can be treated as aperfect capacitor (no dielectric loss), with power being drawn from the transformer. The impedence of the capacitor decreases as the frequency increases. This results in more current being available to the transformer and thus, it generates a higher voltage. When the applied voltage increases to a value close to the breakdown voltage, the power drawn from the power source almost overcomes the saturated transformer loss.

Experimental observations show that if applied voltage on a discharge reactor is rapidly increased, the breakdown frequency is lower than that obtained with a very slow increase in voltage. The magnitude of this effect depend on the rate of rise of voltage with frequency.

In all the tests, a self-sustained discharge of the corona type is observed.

Dry Oxygen Discharges and System Characteristics

The detailed results of non-destructive tests using dry oxygen are given in Appendix A. Appendix B gives the instantaneous variations of primary current, secondary voltages and primary power with frequency at different primary voltages for the various reactors. The voltage increases smoothly with frequency from a low, initial value. At breakdown or corona starting voltage, however, a sudden

or continuous increase of voltage is observed. Further increases in frequency are accompanied by a decrease in the voltage. This is a typical characteristic of an impedance-changing circuit. This is reflected by mostly concave downward curves on figures in Appendix B.

The primary power input reaches a maximum immediately after the gas breaks down. A drastic increase in power input is caused by the build-up of the current flowing in the gap. The energy absorbed in the discharge is drawn from the power source. In the case of reactor A, for a primary voltage of 50 V the primary power input is observed to increase from 7 to 32 W as soon as the breakdown occurs (see Figure 15 in Appendix B). Since the power transferred to the transformer never exceeds 50 W, it appears that more energy dissipates in the power amplifier in order to balance the output. A similar trend is followed by the primary current. The primary current is approximately proportional to the total power input.

CHAPTER VII

RESULTS AND DISCUSSIONS

This chapter describes the preliminary results of the vapor-phase oxidation reaction of titanium tetrachloride in an alternating current plasma reactor. As mentioned earlier, the objective of this study was to check the feasibility of using alternating current plasma reactors for the production of ultrafine powders.

All the experiments were carried out at room temperature and atmospheric pressure. A constant gas flowrate of 1054 ml/minute was maintained in all the experiments except for the case of reactor E, for which it was kept 636 ml/minute because of its smaller annular volume. A corona type discharge was observed on all the reactors used in this work. It is worthwhile to understand the phenomenon (see note in Appendix D).

The ultrafine powders of titanium dioxide were produced using alternating current plasma reactors. The results were obtained by the visual inspection of the transmission electron micrographs (TEM) and the X-ray diffractographs obtained from the Kerr McGee Chemical Corporation. Selected Transmission electron micrographs (TEM) and the X-ray diffractographs are shown in Figures 6-11. The titanium

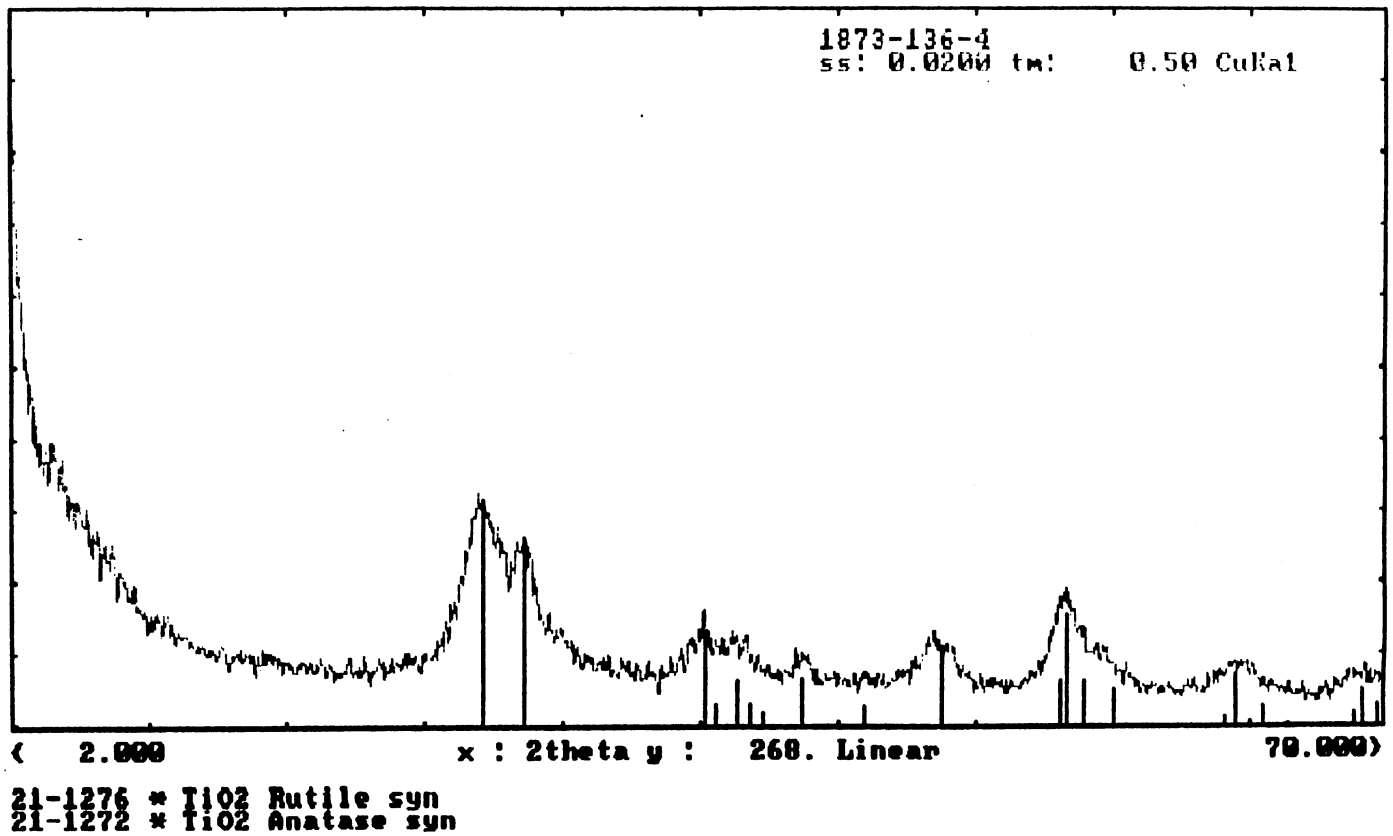

Figure 6. X-Ray Diffractograph for Sample A From Reactor B.

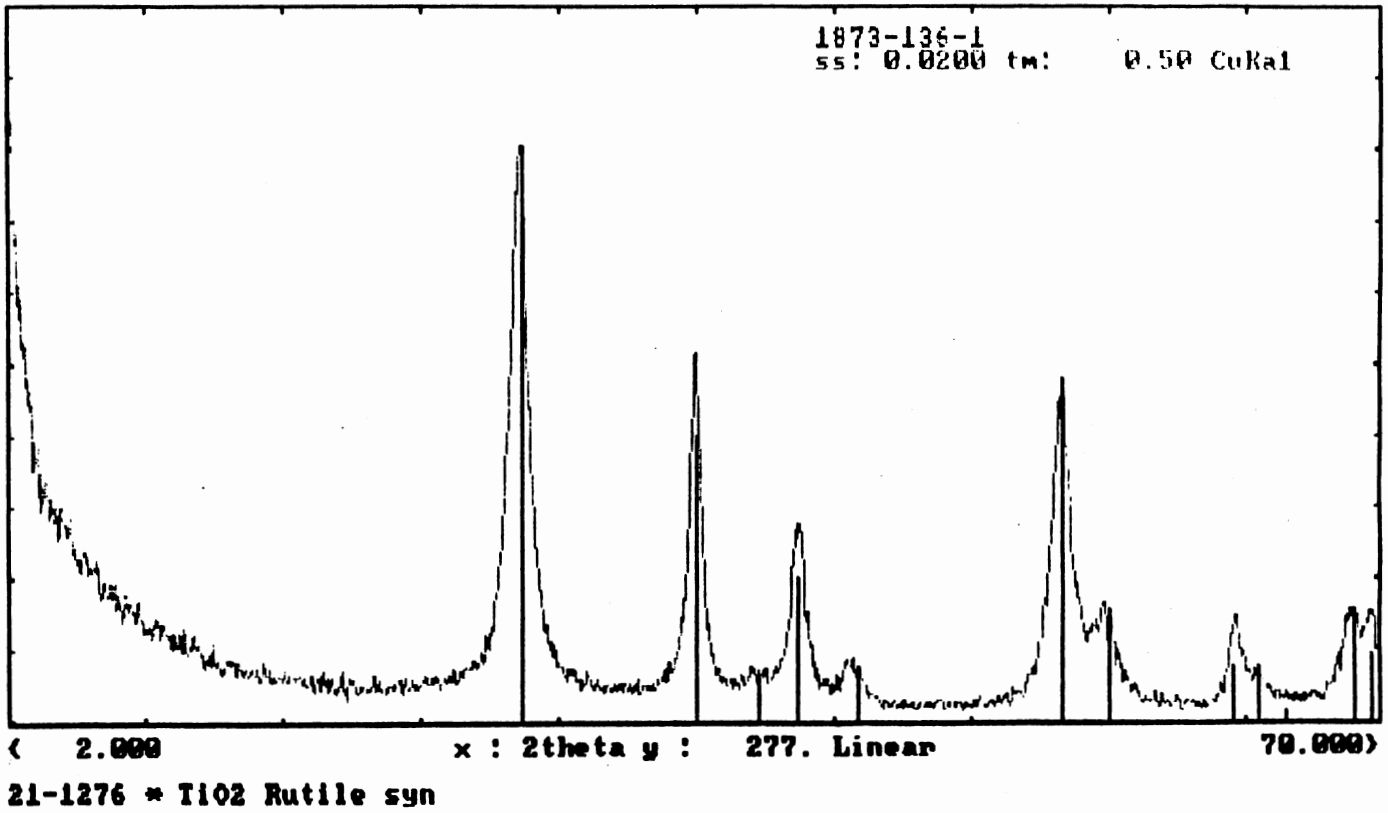

Figure 7. X-Ray Diffractograph for Sample D From Reactor A.

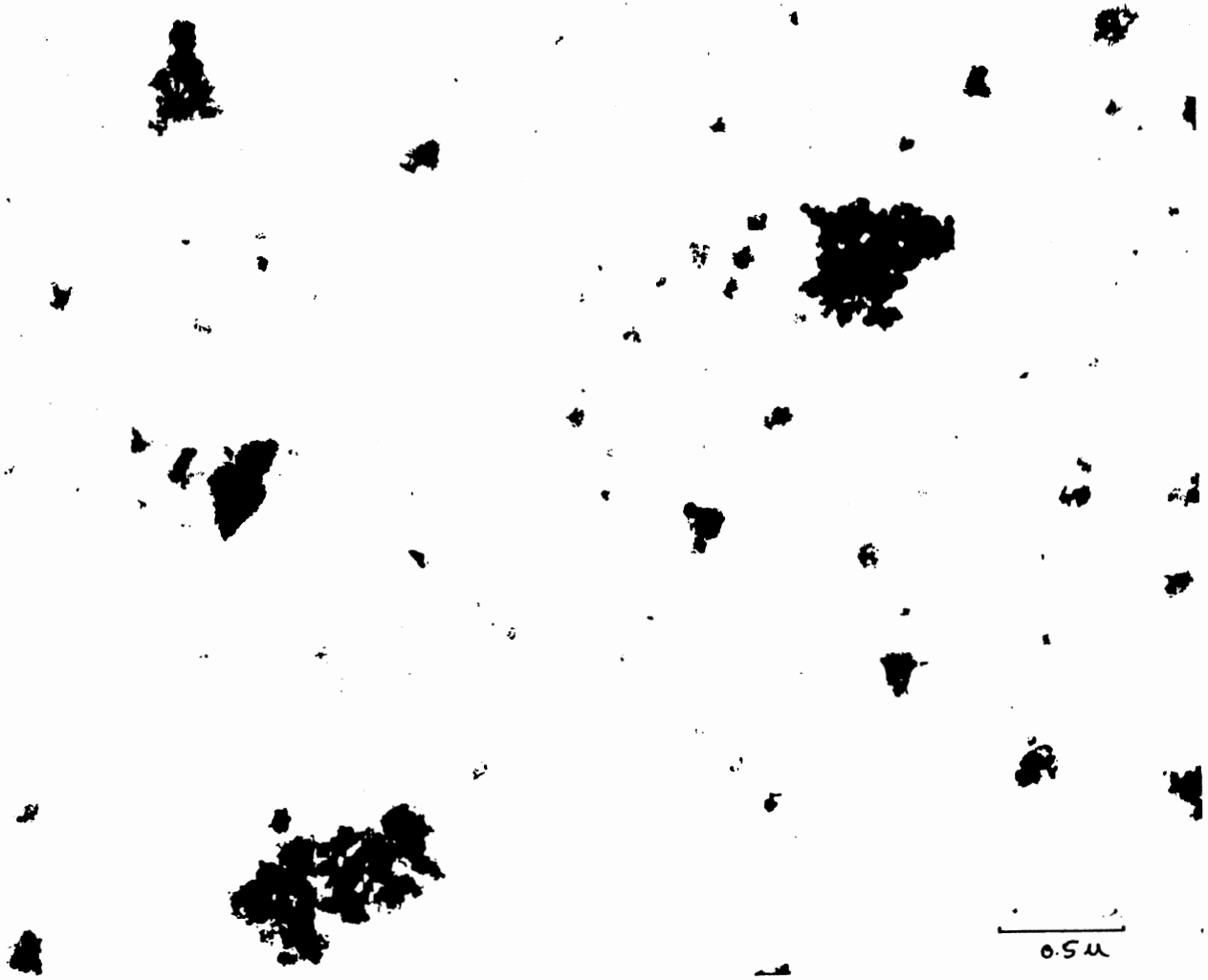

Figure 8. Transmission Electron Micrograph of Sample A From Reactor B.

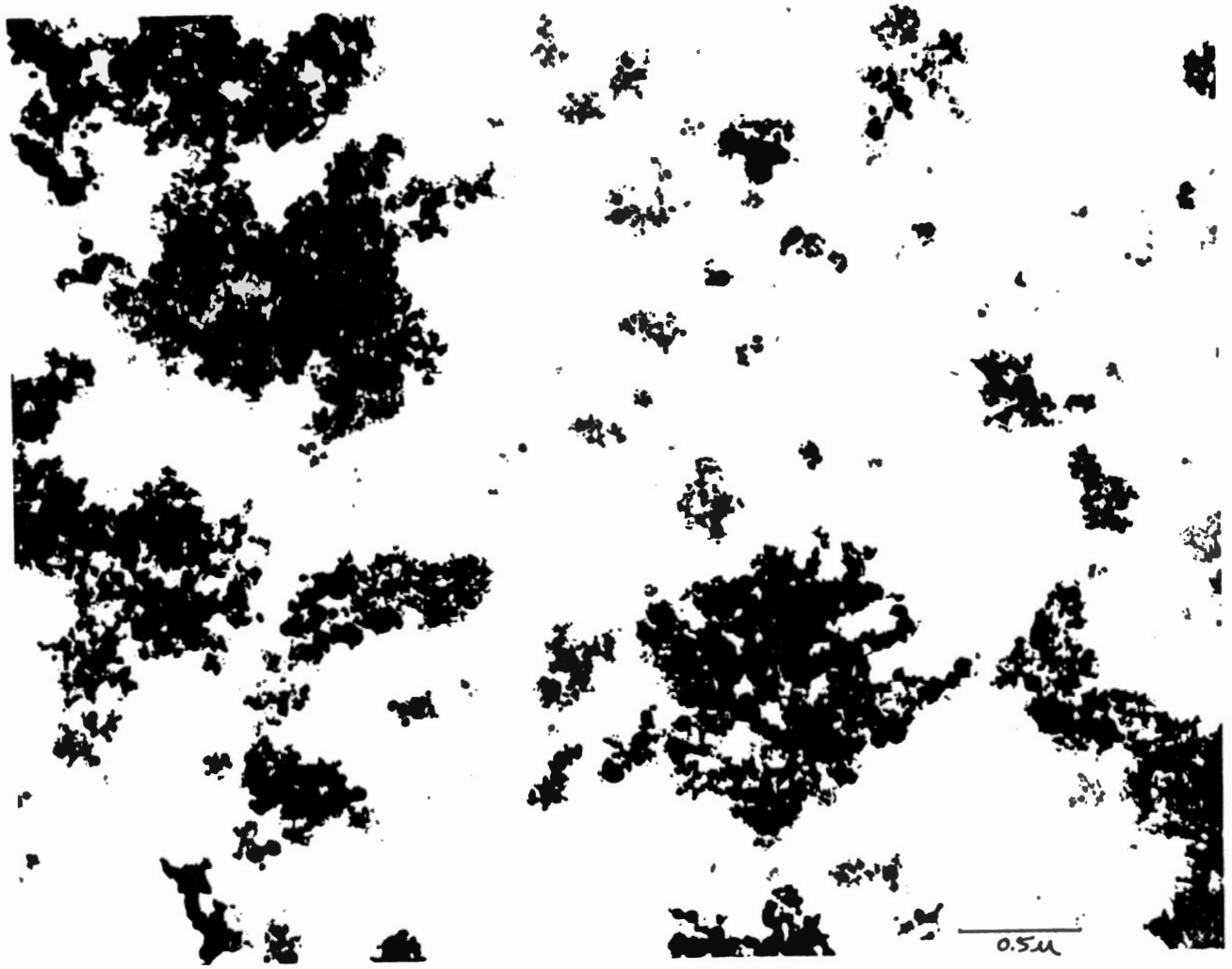

Figure 9. Transmission Electron Micrograph of Sample B From Reactor E.

Figure 11. Transmission Electron Micrograph of Sample D From Reactor A.

dioxide powders produced are snow white and for two samples were a mixture of rutile and anatase two samples were mainly rutile.

Although there exists some agglomerates, the absence of long chain aggregates is noted. The average particle sizes are in the range of 0.001-0.1 μm with a narrow size distribution. The X-ray diffraction patterns yield a large number of distinct lines. In addition to showing that the crystal structure of titanium dioxide powder is rutile or anatase or a mixture of both, the broadening of the lines indicate that the crystalline size is very small (see Figures 6-7). The BET surface area of the different powder samples is in the range 92-160 m^2/gm. The shapes of particles vary from needle-like to spherical. Table V provides a summary of results for four different powder samples from three different runs on reactors A, B and E.

The titanium tetrachloride oxidation reaction is so quick that after a few seconds from the introduction of reactant gases (titanium tetrachloride and oxygen) into the plasma stream, the inside wall of the reactor is covered with a white thick layer of titanium dioxide powder. Due to the speed of the reaction, a significant amount of the product was collected from the reactor by rinsing it with water.

There were problems associated with both powder collection and the tubing used to transfer titanium tetrachloride from flask to the reactor. For the first run,

TABLE V

SUMMARY OF RESULTS FOR DIFFERENT POWDER SAMPLES

	TiO_2 Form	BET Surface Area (m^2/gm)	Residence Time (sec)	Average Particle Size (μm)	Reactor	$TiCl_4$ Conv. %
A]	Rutile Anatase	160	1.3	0.001-0.1	B	63
B]	Rutile Anatase	***	0.34	0.002-0.1	E	59
C]	Rutile	120	2.2	0.001-0.1	A	**
D]	Rutile	92	2.2	0.002-0.1	A	**

** conversion is not available.
*** lack of sample for X-Ray diffraction.

a membrane filter (DM Metricel, from Gelman Sciences) was used. Due to the problem of tremendous pressure drop, this was later changed to a high purity filter (Mathesan, model 6184T4-FF), capable of capturing particles larger than 0.003 μm. For runs 2 and 3 another filter, Polycarbonate Track-Etch (PCTE) membrane filter, obtained from Poretics Corporation, was used, but due to the same problem of pressure drop, the Mathesan filter was used. It is worth mentioning that on all of these runs, none of the samples were collected completely from the filter holder assembly. In other words, each sample was collected in part from the filter and in part from either the reactor outlet port or by rinsing the reactor with water. The samples shown on Table V correspond to the respective runs as follows.

Run 1 - samples C and D (from reactor A)

Run 2 - sample B (from reactor E)

Run 3 - sample A (from reactor B)

Titanium tetrachloride is a highly corrosive material and requires special materials of construction. Teflon tubing was used considering its inert nature, but titanium tetrachloride reacted with it. This is observed by the change in color of Teflon tubing from white to dark brown. This also explains why the conversion on discharge reactor is low.

Figures 12-14 show the variations of primary power, primary current and secondary voltages with frequency for a primary voltage of 40 V, for reactors A, B and E

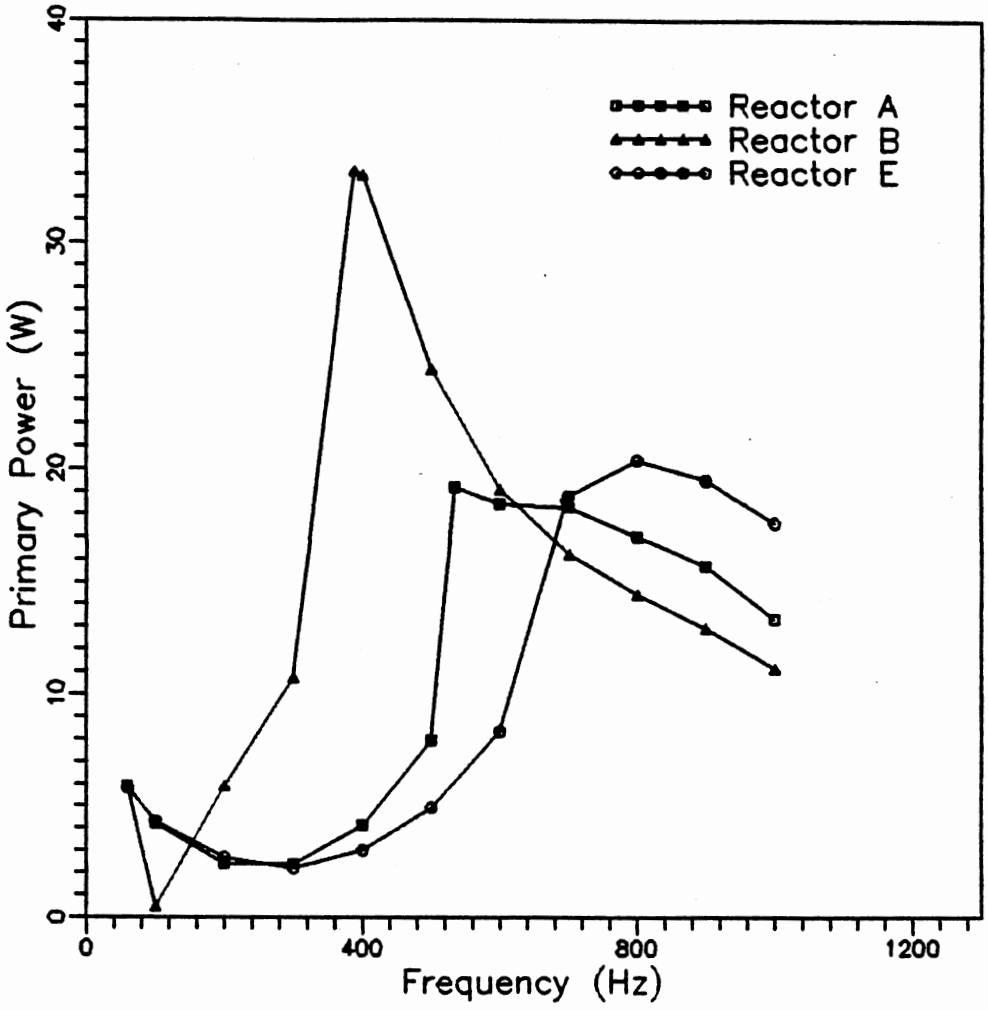

Figure 12. Variation of Primary Power with Frequency for a primary Voltage of 40 V for Reactors A, B and E.

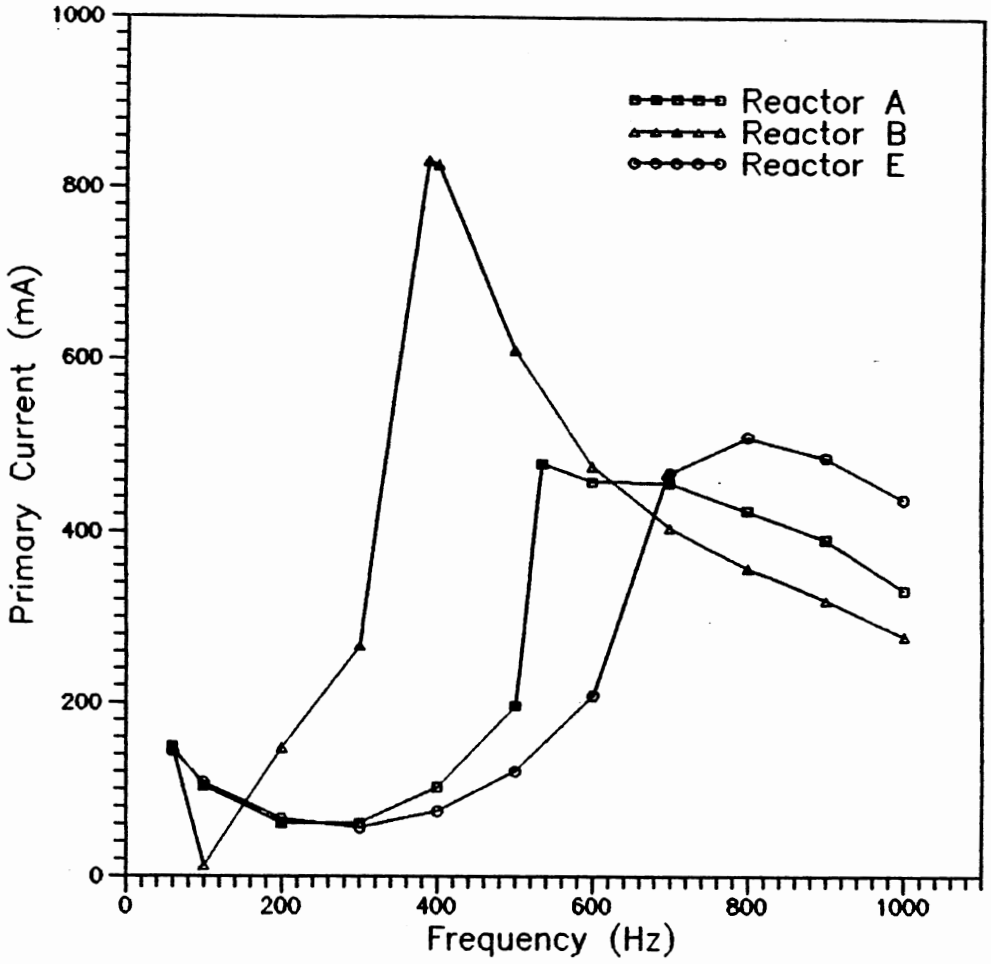

Figure 13. Variation of Primary Current with Frequency for a Primary Voltage of 40 V for Reactors A, B and E.

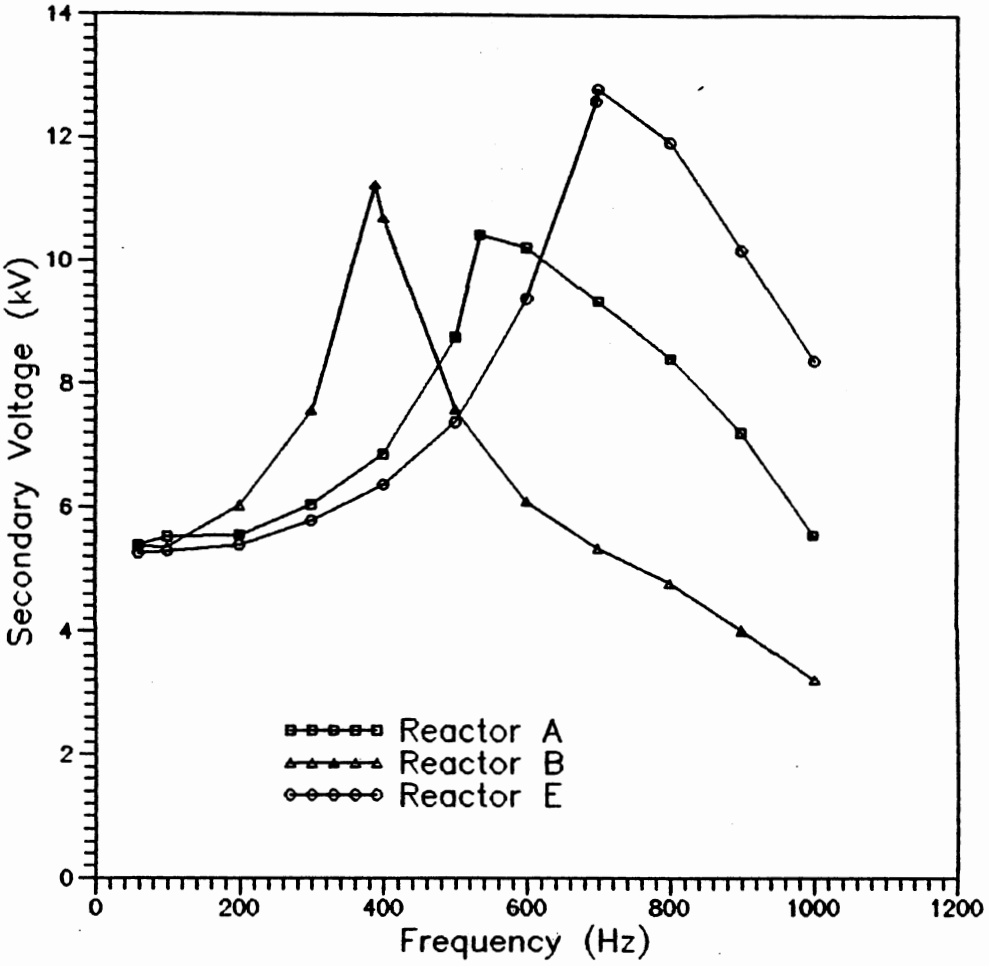

Figure 14. Variation of Secondary Voltage with Frequency for a Primary Voltage of 40 V for Reactors A, B and E.

respectively.

In an impedance-changing discharge system, such as the one used in these experiments, the primary voltage (gain) represents the possible maximum power transferred to the transformer provided that the power factor is assumed to be one. For higher values of primary voltage, higher power input and secondary voltage results. It was observed that for primary voltages of 50 V or higher, an intense glow resulted with arcing. To avoid this, primary voltage of 40 V seemed to be a reasonable choice. Also the maximum rating of the transformer is a limitation. This can be seen clearly in case of reactor B (see Figure 27 in Appendix B).

Reactor B appears to give the best results in terms of surface area, particle size and titanium tetrachloride conversion. The non-destructive data reveal the fact that reactor B has the highest value of primary power input. Another point to note is that reactor B has the smallest gas gap, which results in an intense glow and higher current being available for the discharge.

The product from reactor A is mostly rutile. There may be some traces of anatase, but the X-Ray diffraction pattern showed no evidence of anatase. Reactor A has the longest residence time, it is believed that longer residence time could be one of the reasons for a rutile product. The mechanism of anatase-rutile transformation is a complicated one and is not the goal of this study. However, there is strong evidence in the literature that the reaction of

titanium tetrachloride with oxygen is catalyzed by titanium dioxide particles.

The product from reactor E is a mixture of rutile and anatase particles. The BET surface area is not available because of the lack of enough sample for X-Ray diffraction. Reactor E has the shortest residence time due to the smaller annular area. The conversion in reactor A is not available because these samples were drawn from the very first run and a good record of the original reactant feed amount was impossible due to the system problems. Titanium tetrachloride is highly corrosive and volatile and special materials of construction are required for handling. Although, Teflon tubing was used, considering its inert nature, titanium tetrachloride reacted with this tubing. For this reason, conversion was probably higher than calculated, due to the loss of titanium tetrachloride on the reactor inlet tubing.

CHAPTER VIII

CONCLUSIONS AND RECOMMENDATIONS

Conclusions

From the preliminary results of this work, the following conclusions are drawn:

1. Ultrafine powders of titanium dioxide can be produced using an alternating current plasma reactor.
2. The average particle sizes of titanium dioxide powders are in the range 0.001-0.1 μm with a narrow size distribution. The particle shapes vary from needle-like to spherical.
4. The BET surface area of the produced powders is in the range 90-160 m^2/gm.
5. Homogeneous nucleation followed by condensation growth are believed to be the dominant mechanisms for the formation of ultrafine titanium dioxide powders.
6. In general, the reactor configuration does not seem to have much effect on the particle sizes. However, the effect of smaller gas gap on both the particle shape and surface area is considerable.
7. The lower residence time appears to give more spherical particles and also increased surface area. This is

supported by the samples drawn from the reactors B and E.

8. The higher primary power input appears to have resulted in higher overall conversion and greater surface area. The lower primary power input in case of reactor E, which has comparable product characteristics, is due to the fact that reactor E has the biggest gas gap which requires higher frequency to get a discharge.

Recommendations

The following recommendations are made based on the preliminary results of this study:

1. The problem of handling titanium tetrachloride can be solved by using better materials of construction, so exact calculations on conversion is possible. Nickel tubing is a possible choice.

2. Higher gas flow rates can tried to study the effect of residence time on the reaction products.

3. The use of additives like $AlCl_3$ can be tried. There is strong evidence in the literature that the use of additives results in maximum rutile content.

4. For commercial application of these reactors, the most desirable operating conditions are high flow rates and high pressure. High pressure increases breakdown voltage but reduces gas volume and increases residence time of the gas. The effect of higher pressure must therefore be studied.

5.Detailed characterization of the powder product is needed to examine important features such as size distribution,

fractions of rutile and anatase, and the number density. The DMPS (Differential Mobility Particle Sizer) System in Dr. Johannes's Aerosol Laboratory is capable of doing such an analysis. This system can be used in conjunction with our system, for future studies.

BIBLIOGRAPHY

1. Anderson, H. T., T. Kodas and D. M. Smith. "Vapor-Phase Processing of Powders: Plasma Synthesis and Aerosol Decomposition." Ceramic Bulletin 68(5), 1989: 996-1000.

2. Antipov, I. V., B. G. Koshunov and L. M. Gofman. "Kinetics of the Reaction of Titanium Tetrachloride with Oxygen." Zhurnal Prikladnoi Khimii 40(1), 1967: 11-15.

3. Boenig, H. V. "Plasma Science and Technology." Ithaca: Cornell University Press, 1982.

4. Chen, F. F. "Introduction to Plasma Physics." Ithaca: Cornell University Press, 1974.

5. Coffman, J. A. and W. R. Browne. "Corona Chemistry." Sci. Am. 212(6), 1965: 91-98.

6. Dibelius, N. R., J. C. Fraser, M. Kawahata and C. D. Doyle. "Corona Processing of Coal." Chem. Eng. Prog. 60(6), 1964: 41-44.

7. Dundas, P. H. and M. L. Thorpe,. "Economics and Technology of Chemical Processing with Electric Field Plasmas." Chem. Eng. June 30, 1969: 123-28.

8. Girshick, S. L., C. P. Chiu and P. H. McMurry. "Modelling Particle Formation and Growth in a Plasma Reactor." Plasma Chem. and Plasma Process. 8(2), 1988: 145-157.

9. Johnson, D. W. Jr. "Nonconventional Powder Preparation Technique." Ceramic Bulletin 60(2), 1981: 221-224.

10. Kato, A. and Y. Suyama. "Preparation of Rutile Powders by Vapor Phase Reaction of Ticl4-H2-CO2 System." Chemistry Letters 1974: 961-62.

11. Kaufman, F. "The Production of Atoms and Simple Radicals in Glow Discharges." Advances in Chemistry Series 80, 1969: 29-47.

12. Kingery, W. D. "Introduction to Ceramics." New York: John Wiley & Sons., 1960.

13. Komiyama, H. T. Kanai, and H. Inoue,. "Preparation of

Porous, Amorphous, and Ultrafine TiO2 Particles by Chemical Vapor Deposition." Chemistry Letters 1984: 1283-86.

14. Kuhn, W. E. "Ultrafine Particles." New York: John Wiley & Sons, Inc., 1963.

15. Loeb, L. B. "Fundamental Processes of Electrical Discharges in Gases." New York: John Wiley & Sons, Inc., 1939.

16. Mahawili, I. and F. J. Weinberg. "A Study of TiCl4 Oxidation in a Rotating Arc Plasma Jet." 1979. A.I.Ch.E. Symposium Series 75.

17. Matijevic, E. Budnik, M. and L. Meites. "Preparation and Mechanism of Formation of Titanium Dioxide Hydrosols of Narrow Size Distributions." J. Colloid Interface Sci. 44(2) 1977: 302-11.

18. Morooka, S. A. Kobata, T. Umeda, and K. Kusakabe. "Average Size and Rutile Content of TiO2 Particles Produced by Oxidation of TiCl4 without additive in Aerosol Reactors." J. Chem. Eng. Jpn. 221 (1989): 94-6.

19. Musa, G. C. P. Ionescu, I. Lungu, S. Mustata, I. C. Popa, and O. Seicaru. "Plasma Production of TiO2 from $TiCl_4$." Contrib. Plasma Phys. 27(3), 1987: 181-86.

20. Nicholson, P. S. "Primary and Secondary Advanced Ceramic Powder Processing." Proceedings of the International Symposium. " 1988. 533-543.

21. Parker, I. M. "A Thermodynamics Analysis of the Production of TiO2 from Ticl4." Chemistry & Industry (1972):

22. Schnell, C. R., S. M. L. Hamblyn, K. Hengartner and M. Wissler. "The Industrial Application of Plasma Technology for the Production of Fumed Silica." Powder Technology 20.(1978): 15-20.

23. Suyama, Y. K. Ito, and A. Kato. "Mechanism of Rutile Formation in Vapor Phase Oxidation of TiCl4 by Oxygen." J.Inorg. Nucl. Chem. 37, 1975: 1883-88.

24. Suyama, Y. and A. Kato. "TiO2 Produced by Vapor Phase Oxygenolysis of TiCl4." J. Am. Ceram. Soc. 59(3-4), 1976:146-49.

25. Thomas, C. L., Egloff, G. and J. C. Morrel. "Reactions of Hydrocarbons in Electrical Discharges." Chem. Revs. 28, 1941:

26. Thorpe, M. L. Jr. and P. H. Wilks. "Electric-Arc Furnace Turns Zircon Sand to Zirconia." Chem. Eng. 1971: 117-19.

27. Thorpe, M. "Plasma Energy: the Ultimate in Heat Transfer." Chem. Eng. Prog. 85.7 (1989): 43-53.

28. Tsai, V. Y. Conceptual Design and Performance Analysis of Frequency-Tuned Capacitive Discharge Reactors. Ph.D Dissertation, Oklahoma State University, Stillwater, Oklahoma. (1991).

29. Visca, M. and E. Matijevic. "Preparation of Uniform Colloidal Dispersion by Chemical Reaction in Aerosols." J.Colloid Int. Sci. 68(2), (1979): 308-319.

30. Waddie, B. "Review of Recent Work on the Processing of Powders in High Temperature Plasmas. Part I." Chem. Engr. 259, 1972: 92-6.

31. Warren, D. R. and J. H. Seinfeld. "Nucleation and Growth of Aerosol from a Continuously Reinforced Vapor." Aerosol Sci. Technol. 3, 1984: 135-153

32. Wilks, P. H. and M. L. Thorpe. "Titanium Dioxide Production by Plasma Processing." Chem. Eng. Prog. 68(4), 1972: 82-3.

33. Young, R. M. and E. Pfender,. "Generation and Behavior of Fine Particles in Thermal Plasma - A Review." Plasma Chem. Plasma Process. 5, 1985: 1-37.

APPENDICES

APPENDIX A

EXPERIMENTAL DATA

TABLE VI

NON-DESTRUCTIVE TEST

Reactor: A			Status: instantaneous	
Gas: Dry Oxygen			Flowrate: 1054 ml/min	
Vp (V)	f (Hz)	Ip (mA)	Vs (V)	Wp (W)
20	60	112	3400	2.2
	100	81	3440	1.6
	200	43	2740	0.9
	300	26	2920	0.5
	400	37	3300	0.7
	500	73	4040	1.5
	600	147	5620	2.9
	700	334	8380	6.7
	729	355	8200	7.1
	800	367	5800	7.3
	900	300	3160	6.0
	1000	193	8780	3.9
30	60	125	4040	3.7
	100	89	4050	2.7
	200	53	4050	1.6
	300	39	4400	1.2
	400	64	4900	1.9
	500	120	6080	3.6
	600	270	9120	8.1
	640	375	9240	11.3
	700	395	9230	11.8
	800	390	8440	11.7
	900	363	7200	10.9
	1000	249	4360	7.5
40	60	149	5400	5.9
	100	104	5540	4.2
	200	61	5560	2.4
	300	61	6060	2.4
	400	103	6880	4.1
	500	197	8780	7.9
	535	480	10440	19.2
	600	459	10240	18.4
	700	458	9360	18.3
	800	426	8440	17.0
	900	393	7240	15.7
	1000	333	5580	13.3

TABLE VI (Continued)

Vp (V)	f (Hz)	Ip (mA)	Vs (V)	Wp (W)
50	60	174	6760	8.7
	100	117	6800	5.9
	200	74	6980	3.7
	300	81	7640	4.0
	400	136	8780	6.8
	420	636	10880	31.8
	500	714	11000	35.7
	600	573	9580	28.6
	700	495	8600	24.8
	800	447	7800	22.4
	900	408	6800	20.4
	1000	369	5640	18.5

TABLE VII

NON-DESTRUCTIVE TEST

Reactor: B			Status: instantaneous	
Gas: Dry Oxygen			Flowrate: 1054 ml/min	
Vp (V)	f (Hz)	Ip (mA)	Vs (V)	Wp (W)
20	60	100	2760	2.0
	100	70	2770	1.4
	200	36	2780	0.7
	300	31	3160	0.6
	400	65	3680	1.3
	500	140	5160	2.8
	552	309	6120	6.2
	600	312	5960	6.2
	700	301	5400	6.0
	800	272	4760	5.4
	900	194	2900	3.9
	1000	142	1700	2.8
30	60	120	4000	3.6
	100	84	4040	2.5
	200	46	4120	1.4
	300	55	4600	1.6
	400	112	5600	3.3
	440	579	8820	17.4
	500	507	7660	15.2
	600	413	6380	12.4
	700	368	5780	11.1
	800	327	5000	9.8
	900	288	4100	8.6
	1000	211	2460	6.3
40	60	148	5380	5.9
	100	12	5360	0.5
	200	148	6040	5.9
	300	267	7580	10.7
	388	831	11240	33.2
	400	826	10700	33.0
	500	611	7600	24.4
	600	477	6120	19.1
	700	406	5360	16.2
	800	359	4800	14.4
	900	321	4040	12.9
	1000	279	3220	11.1

TABLE VII (Continued)

Vp (V)	f (Hz)	Ip (mA)	Vs (V)	Wp (W)
50	60	175	6760	8.7
	100	150	6780	7.5
	200	223	7640	11.2
	300	519	11000	25.9
	325	894	15000	44.7

TABLE VIII

NON-DESTRUCTIVE TEST

Reactor: C			Status: instantaneous	
Gas: Dry Oxygen			Flowrate: 1054 ml/min	
Vp (V)	f (Hz)	Ip (mA)	Vs (V)	Wp (W)
20	60	102	2760	2.0
	100	73	2760	1.5
	200	41	2780	0.8
	300	25	2920	0.5
	400	38	3280	0.8
	500	73	4000	1.5
	600	148	5600	3.0
	700	360	9600	7.2
	708	378	9720	7.6
	800	384	8820	7.7
	900	279	5600	5.6
	1000	170	2840	3.4
30	60	123	4020	3.7
	100	88	4040	2.6
	200	54	4060	1.6
	300	40	4400	1.2
	400	64	4960	1.9
	500	121	6060	3.6
	600	237	8760	7.1
	668	441	10560	13.2
	700	459	10440	13.8
	800	455	9200	13.6
	900	415	7560	12.5
	1000	279	4200	8.4
40	60	147	5390	5.9
	100	102	5400	4.1
	200	63	5580	2.5
	300	60	6220	2.4
	400	102	6880	4.1
	500	180	8520	7.2
	585	499	11000	20.0
	600	508	10960	20.3
	700	510	10060	20.4
	800	488	9000	19.5
	900	446	7400	17.9
	1000	360	5400	14.4

TABLE VIII (Continued)

Vp (V)	f (Hz)	Ip (mA)	Vs (V)	Wp (W)
50	60	174	6780	8.7
	100	117	6800	5.8
	200	75	7040	3.7
	300	82	7680	4.1
	400	137	8820	6.9
	478	696	12400	34.8
	500	704	12200	35.2
	600	624	10760	31.2
	700	566	9620	28.3
	800	539	8660	27.0
	900	482	7380	24.1
	1000	430	6360	21.5

TABLE IX

NON-DESTRUCTIVE TEST

Reactor: D			Status: instantaneous	
Gas: Dry Oxygen			Flowrate: 1054 ml/min	
Vp (V)	f (Hz)	Ip (mA)	Vs (V)	Wp (W)
20	60	100	2700	2.0
	100	73	2740	1.5
	200	38	2780	0.8
	300	26	3020	0.5
	400	48	3440	1.0
	500	98	4400	2.0
	600	204	7000	4.1
	700	363	8380	7.3
	710	360	7800	7.2
	800	342	7240	6.8
	900	216	4080	4.3
	1000	165	2380	3.3
30	60	122	4000	3.7
	100	86	4020	2.6
	200	50	4140	1.5
	300	44	4520	1.3
	400	83	5240	2.5
	500	164	6880	4.9
	600	420	8820	12.6
	622	431	9000	12.9
	700	428	8180	12.8
	800	384	7400	11.5
	900	324	5780	9.7
	1000	216	3300	6.5
40	60	145	5320	5.8
	100	100	5390	4.0
	200	65	5800	2.6
	300	75	6600	3.0
	400	137	7760	5.5
	437	633	10400	25.3
	500	588	9380	23.5
	600	537	8640	21.5
	700	471	7800	18.8
	800	420	7000	16.8
	900	378	6000	15.1
	1000	312	4500	12.5

TABLE IX (Continued)

Vp (V)	f (Hz)	Ip (mA)	Vs (V)	Wp (W)
50	60	171	6800	8.6
	100	113	6800	5.6
	200	76	7220	3.8
	300	98	8000	4.9
	400	828	10900	41.4
	500	768	10000	38.4
	600	659	9200	32.9
	700	558	8200	27.9
	800	500	7620	25.0
	900	447	6500	22.4
	1000	396	5440	19.8

TABLE X

NON-DESTRUCTIVE TEST

Reactor: E			Status: instantaneous	
Gas: Dry Oxygen			Flowrate: 1054 ml/min	
Vp (V)	f (Hz)	Ip (mA)	Vs (V)	Wp (W)
20	60	105	2640	2.1
	100	77	2680	1.5
	200	46	2600	0.9
	300	31	2840	0.6
	400	31	3020	0.6
	500	49	3500	1.0
	600	83	4300	1.7
	700	152	5800	3.0
	800	347	10100	6.9
	825	378	10340	7.6
	900	382	9160	7.6
	1000	375	5540	7.5
30	60	126	3960	3.8
	100	93	3940	2.8
	200	60	3980	1.8
	300	42	4200	1.3
	400	49	4600	1.5
	500	76	5280	2.3
	600	137	6680	4.1
	700	260	9640	7.8
	760	406	11540	12.2
	800	445	11440	13.4
	900	442	9700	13.2
	1000	383	7600	11.5
40	60	144	5260	5.8
	100	108	5300	4.3
	200	66	5400	2.7
	300	56	5800	2.2
	400	75	6380	3.0
	500	121	7400	4.9
	600	209	9400	8.3
	697	465	12600	18.6
	700	469	12800	18.8
	800	511	11940	20.4
	900	487	10200	19.5
	1000	439	8400	17.6

TABLE X (Continued)

Vp (V)	f (Hz)	Ip (mA)	Vs (V)	Wp (W)
50	60	177	6700	8.9
	100	121	6760	6.0
	200	77	6840	3.8
	300	74	7400	3.7
	400	105	8200	5.3
	500	170	9600	8.5
	600	421	13240	21.0
	635	560	14000	28.0
	700	585	13800	29.2
	800	582	12460	29.1
	900	559	10600	27.9
	1000	488	8960	24.4

TABLE XI

NON-DESTRUCTIVE TEST

Reactor: F			Status: instantaneous	
Gas: Dry Oxygen			Flowrate: 1054 ml/min	
Vp (V)	f (Hz)	Ip (mA)	Vs (V)	Wp (W)
20	60	105	2660	2.1
	100	78	2700	1.6
	200	49	2580	1.0
	300	30	2760	0.6
	400	23	2840	0.5
	500	29	3160	0.6
	600	46	3620	0.9
	700	74	4360	1.5
	800	127	5680	2.5
	900	261	8820	5.2
	920	291	9100	5.8
	1000	312	8200	6.2
30	60	129	4000	3.9
	100	94	3800	2.8
	200	58	3700	1.7
	300	39	4120	1.2
	400	36	4420	1.1
	500	51	4840	1.5
	600	81	5600	2.4
	700	130	6880	3.9
	800	252	9800	7.6
	880	443	12780	13.3
	900	455	12560	13.6
	1000	402	9640	12.1
40	60	146	5320	5.9
	100	110	5280	4.4
	200	74	5320	3.0
	300	53	5560	2.1
	400	51	5800	2.0
	500	72	6580	2.9
	600	113	7600	4.5
	700	200	9700	8.0
	800	493	15440	19.7
	900	*	*	*
	1000	*	*	*

TABLE IX (Continued)

Vp (V)	f (Hz)	Ip (mA)	Vs (V)	Wp (W)
50	60	183	6760	9.2
	100	125	6800	6.3
	200	84	6800	4.2
	300	63	7040	3.2
	400	68	7600	3.4
	500	101	8420	5.0
	600	171	10040	8.6
	700	344	13780	17.2
	720	414	15220	20.7
	800	*	*	*
	900	*	*	*
	1000	*	*	*

APPENDIX B

NON-DESTRUCTIVE TESTS RESULTS

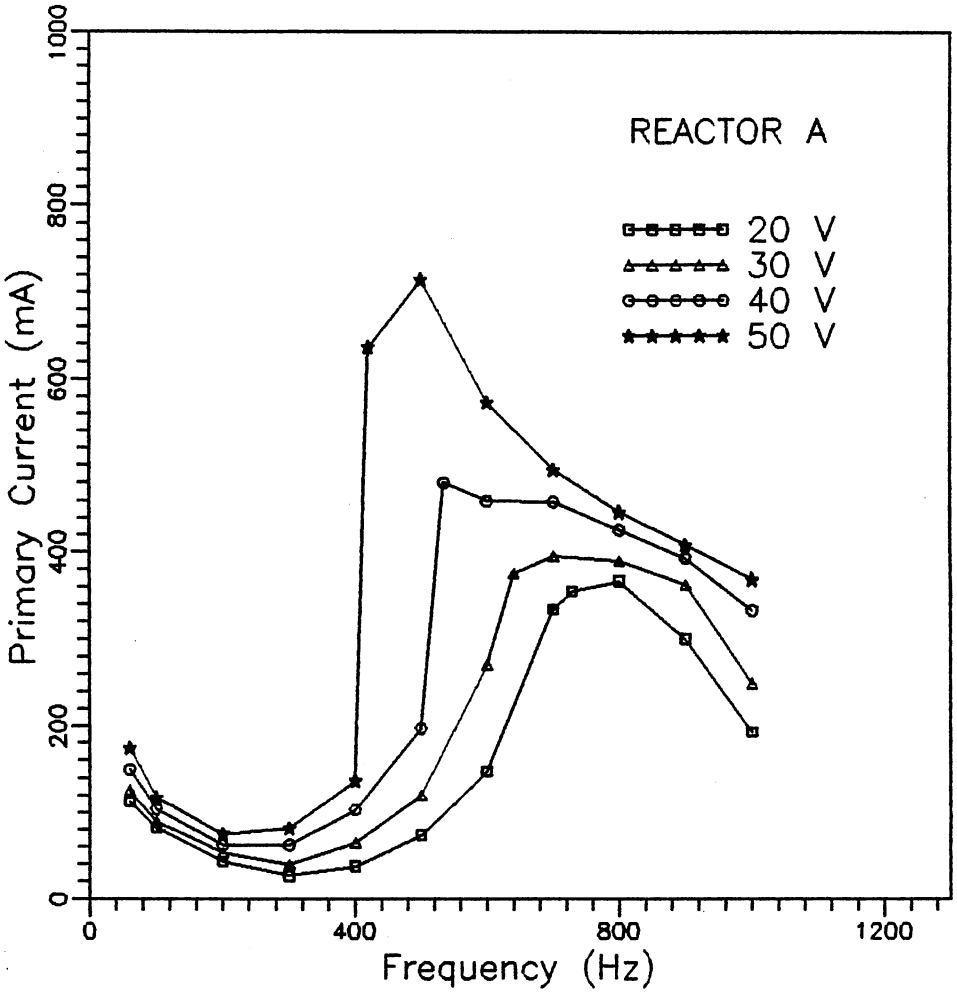

Figure 15. Variation of Primary Current with Frequency and Primary Voltage for Reactor A.

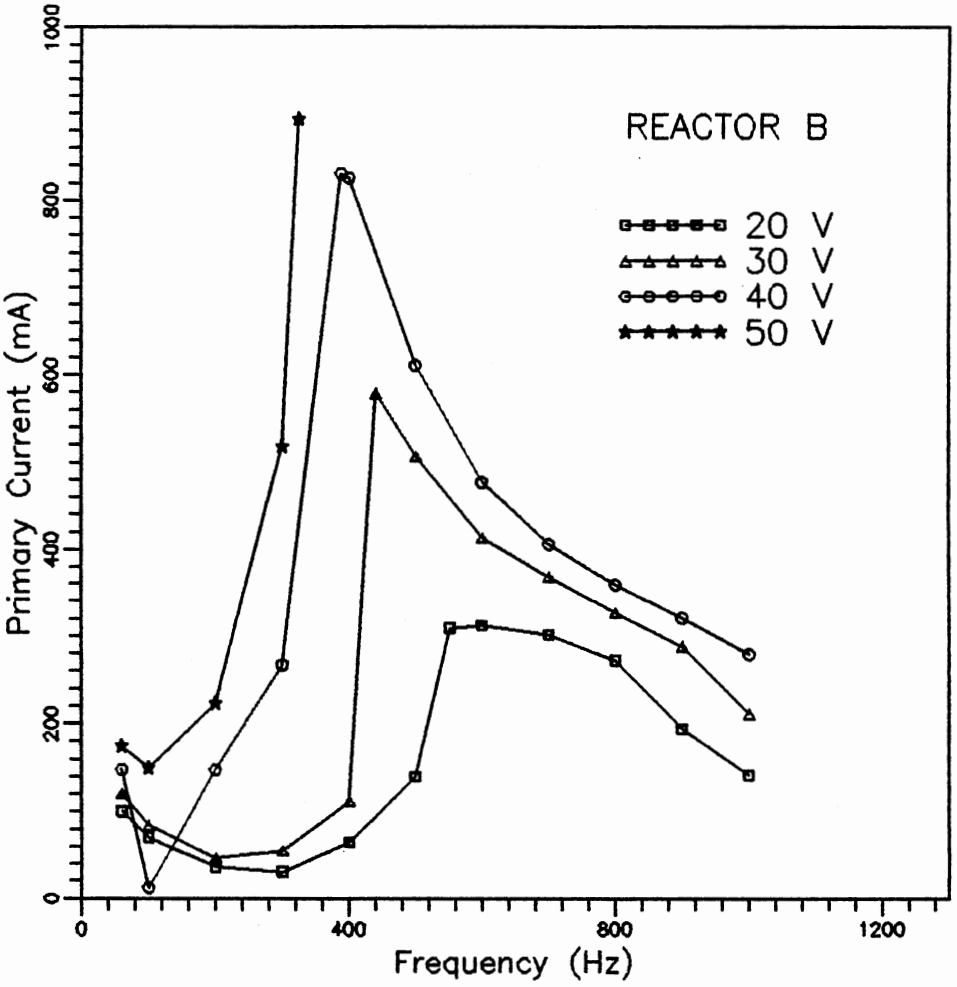

Figure 16. Variation of Primary Current with Frequency and Primary Voltage for Reactor B.

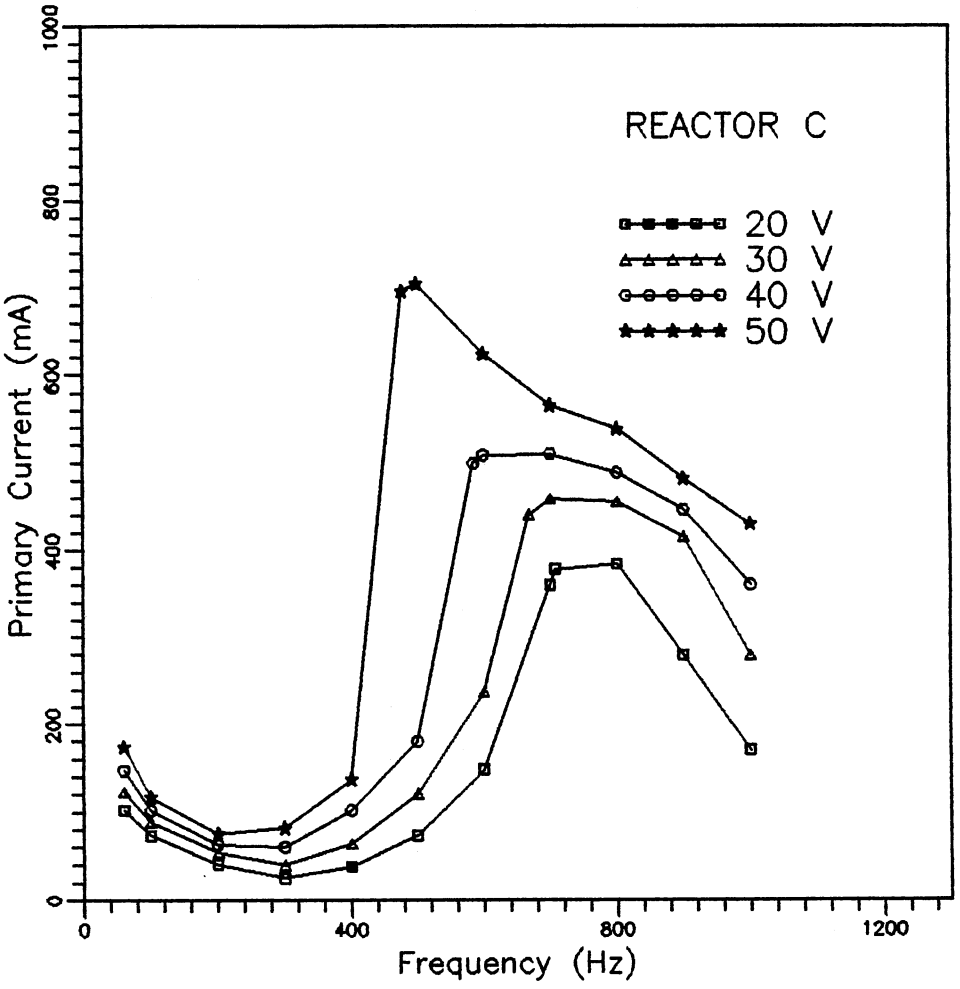

Figure 17. Variation of Primary Current with Frequency and Primary Voltage for Reactor C.

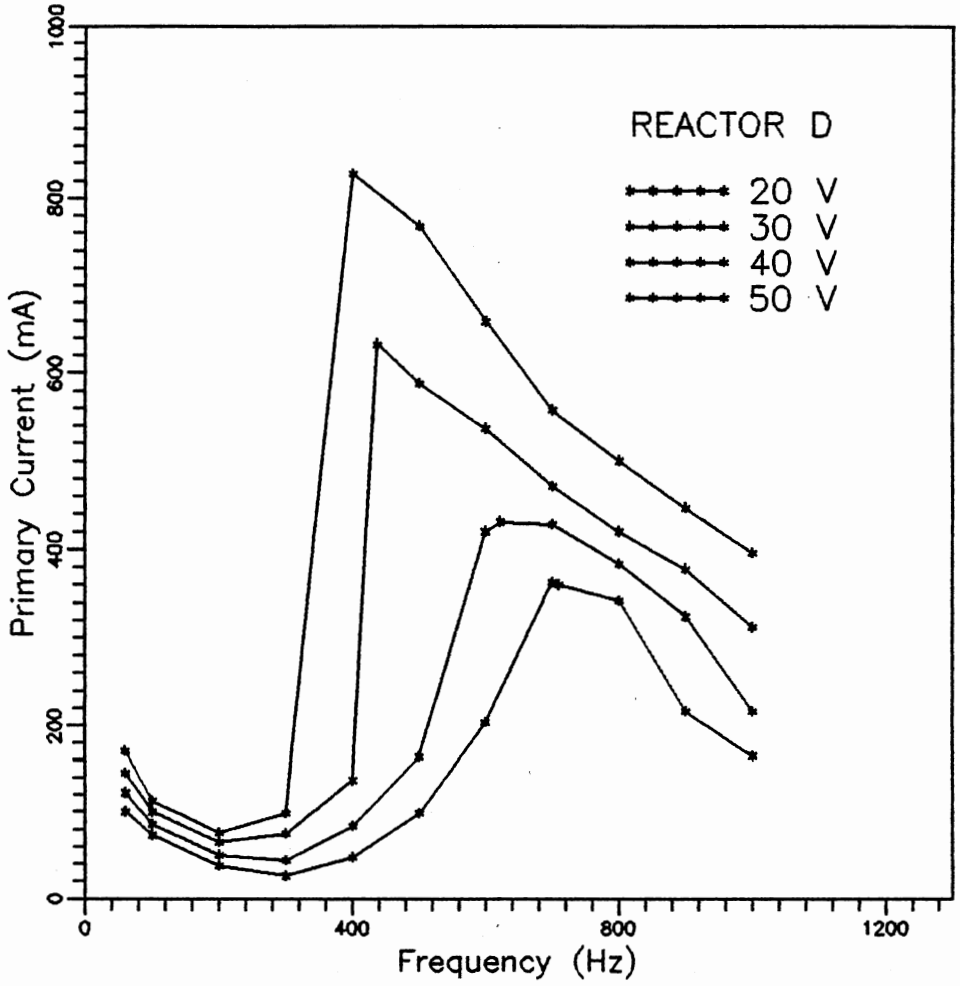

Figure 18. Variation of Primary Current with Frequency and Primary Voltage for Reactor D.

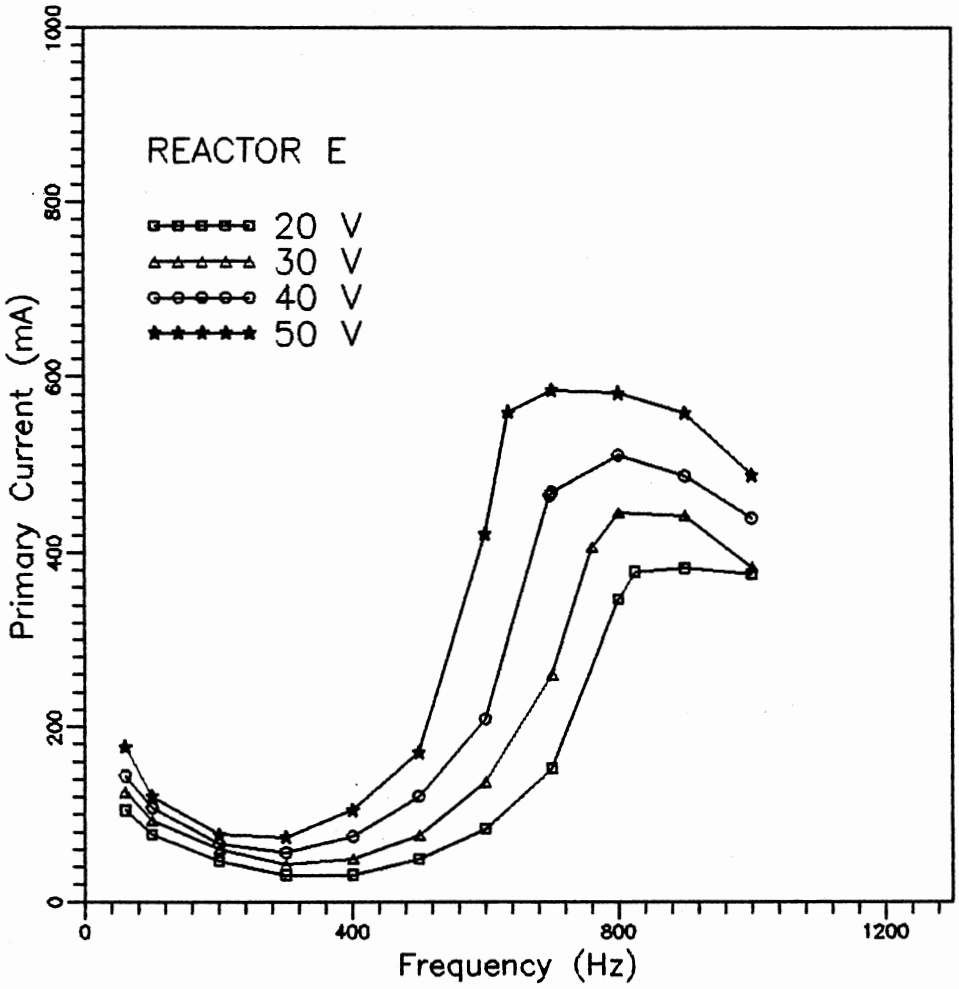

Figure 19. Variation of Primary Current with Frequency and Primary Voltage for Reactor E.

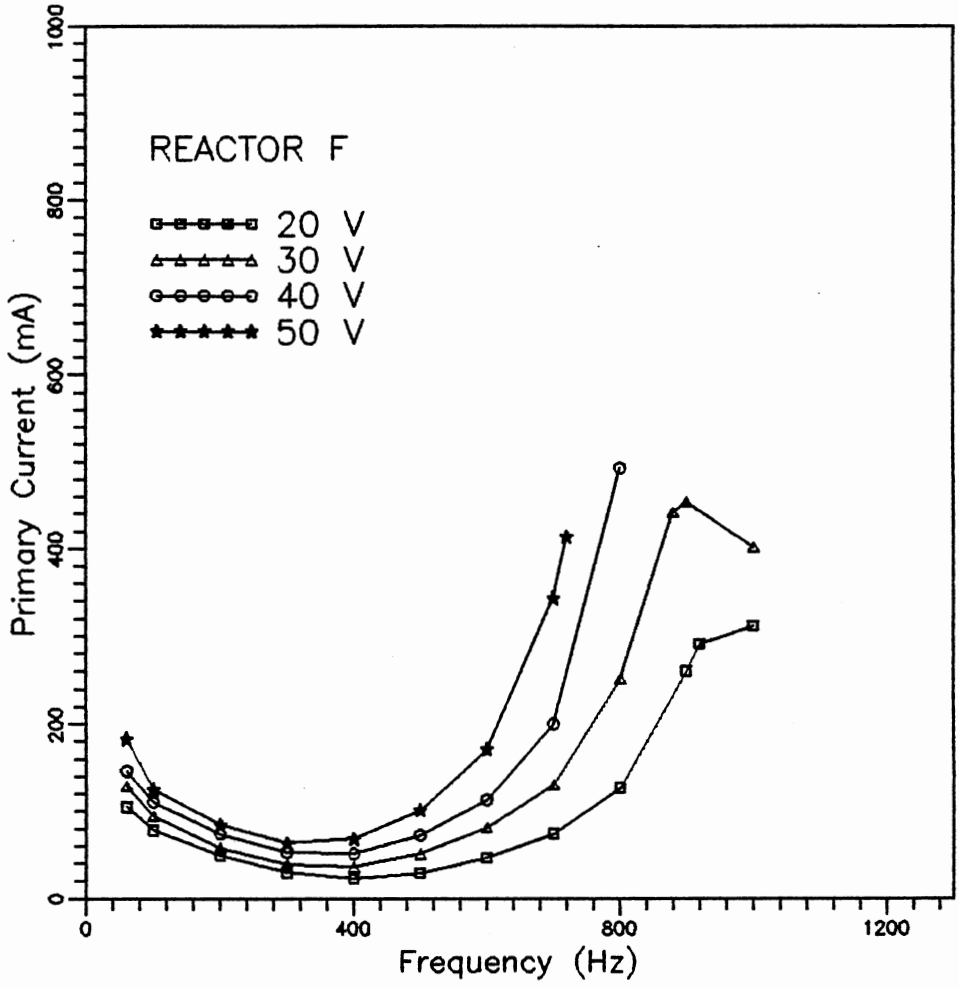

Figure 20. Variation of Primary Current with Frequency and Primary Voltage for Reactor F.

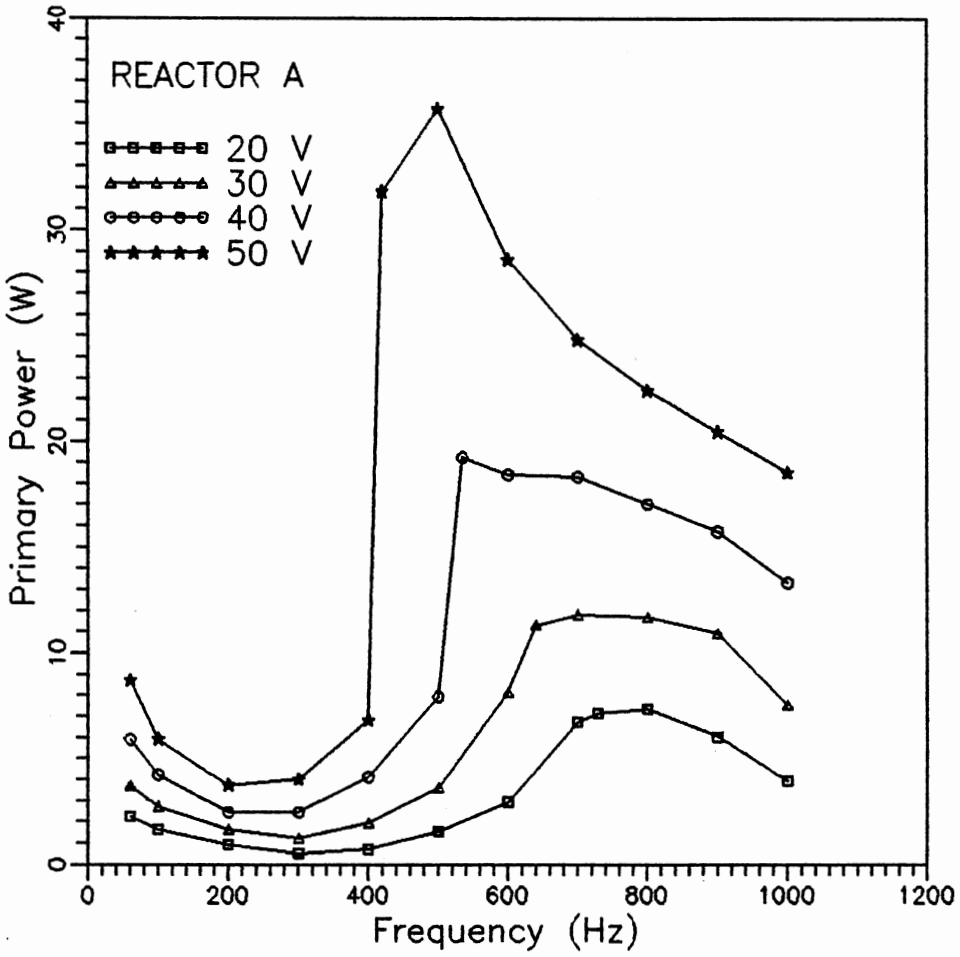

Figure 21. Effect of Frequency and Primary Voltage on Primary Power for Reactor A.

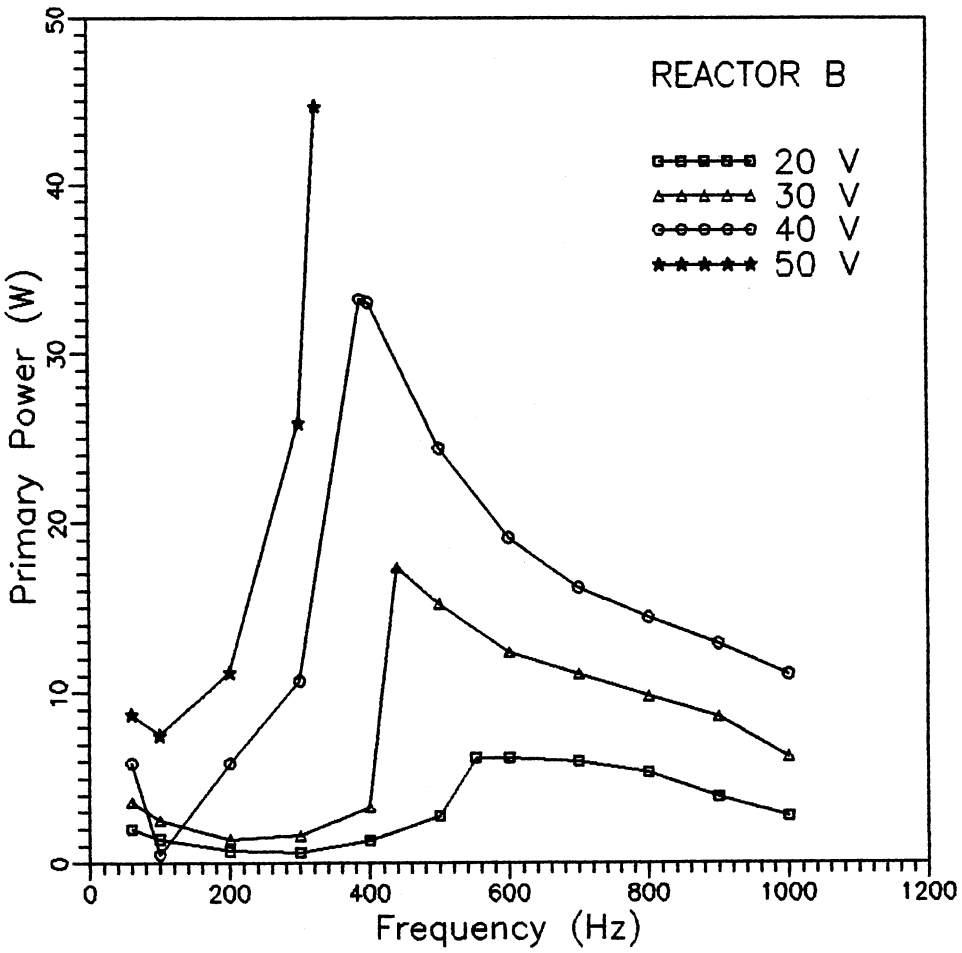

Figure 22. Effect of Frequency and Primary Voltage on Primary Power for Reactor B.

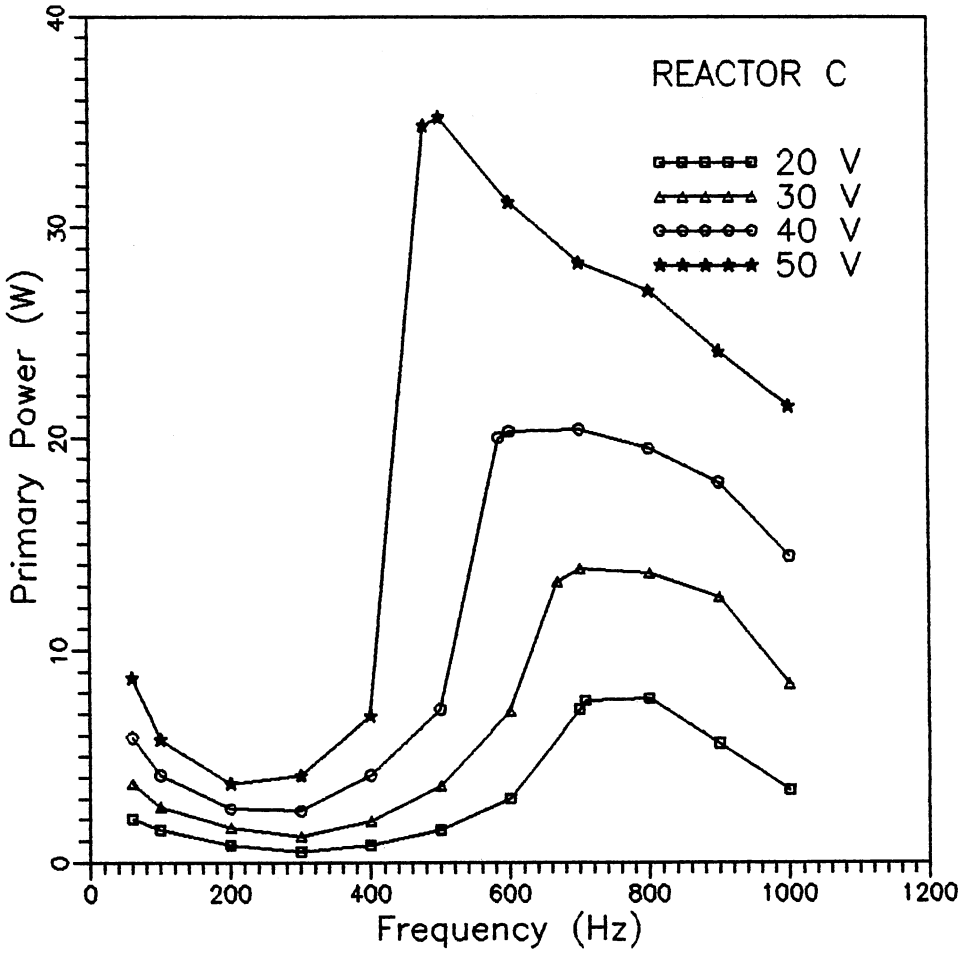

Figure 23. Effect of Frequency and Primary Voltage on Primary Power for Reactor C.

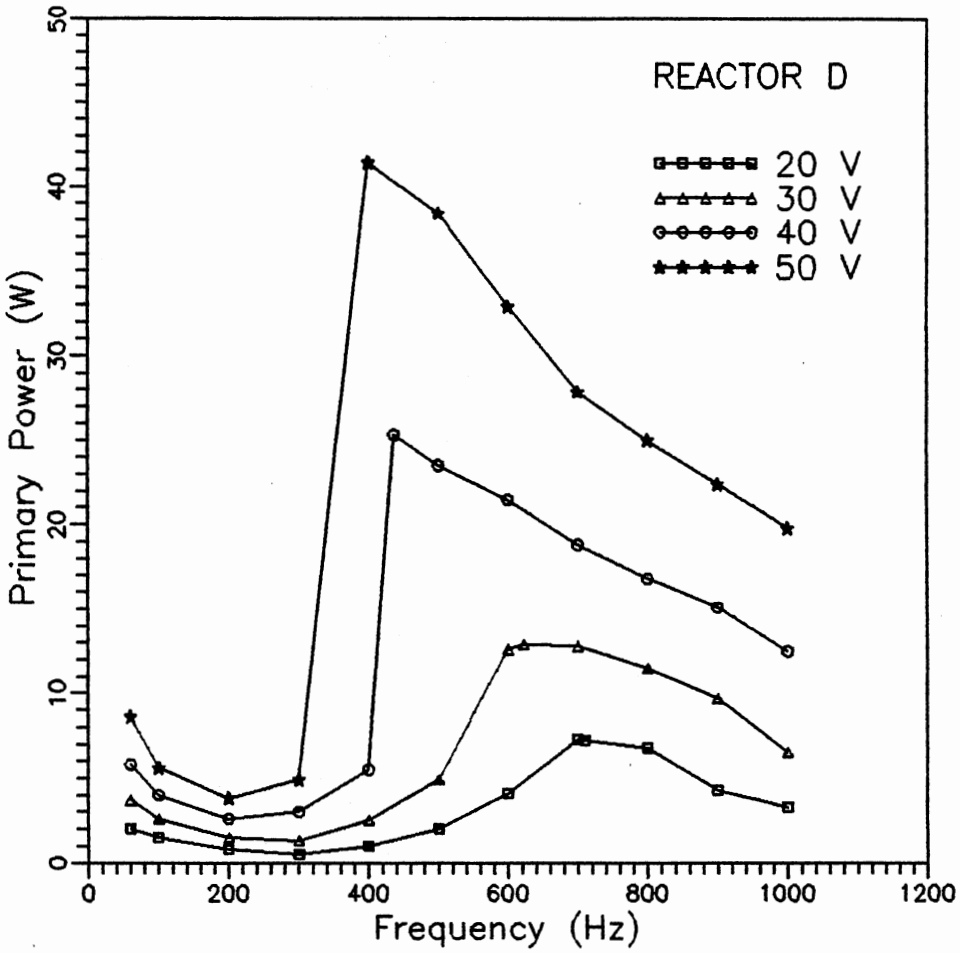

Figure 24. Effect of Frequency and Primary Voltage on Primary Power for Reactor D.

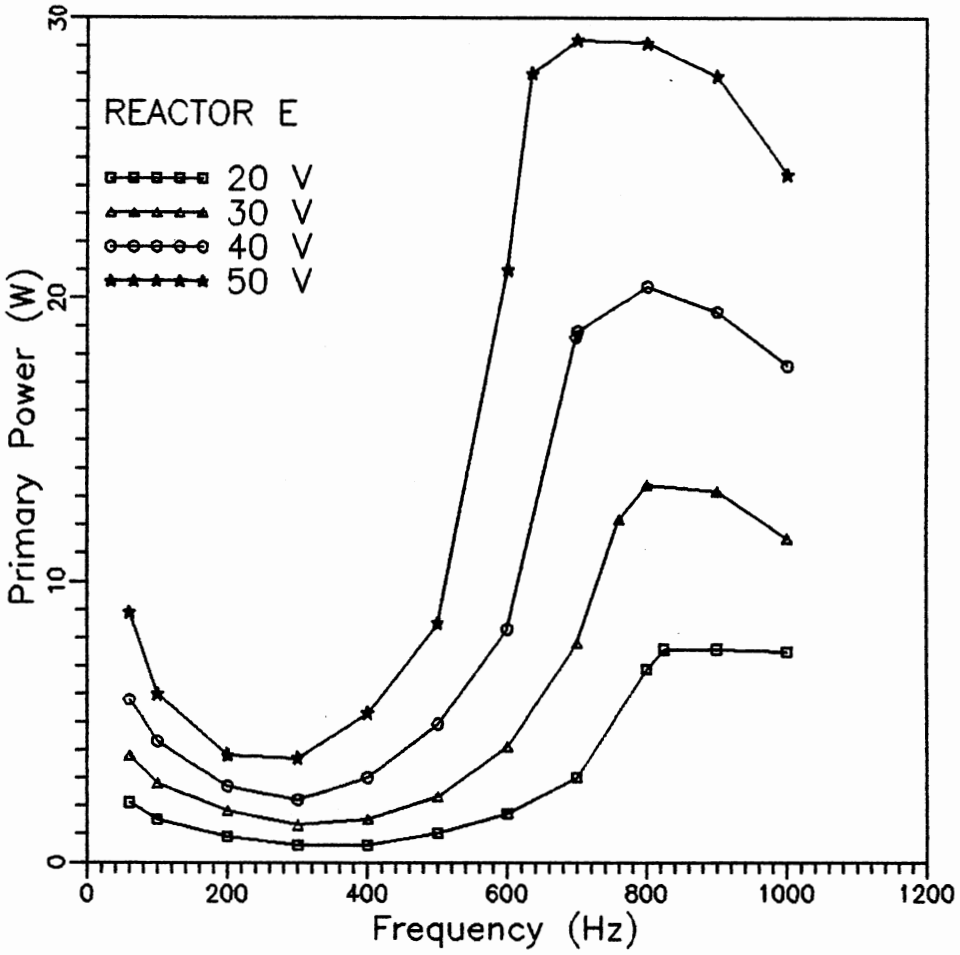

Figure 25. Effect of Frequency and Primary Voltage on Primary Power for Reactor E.

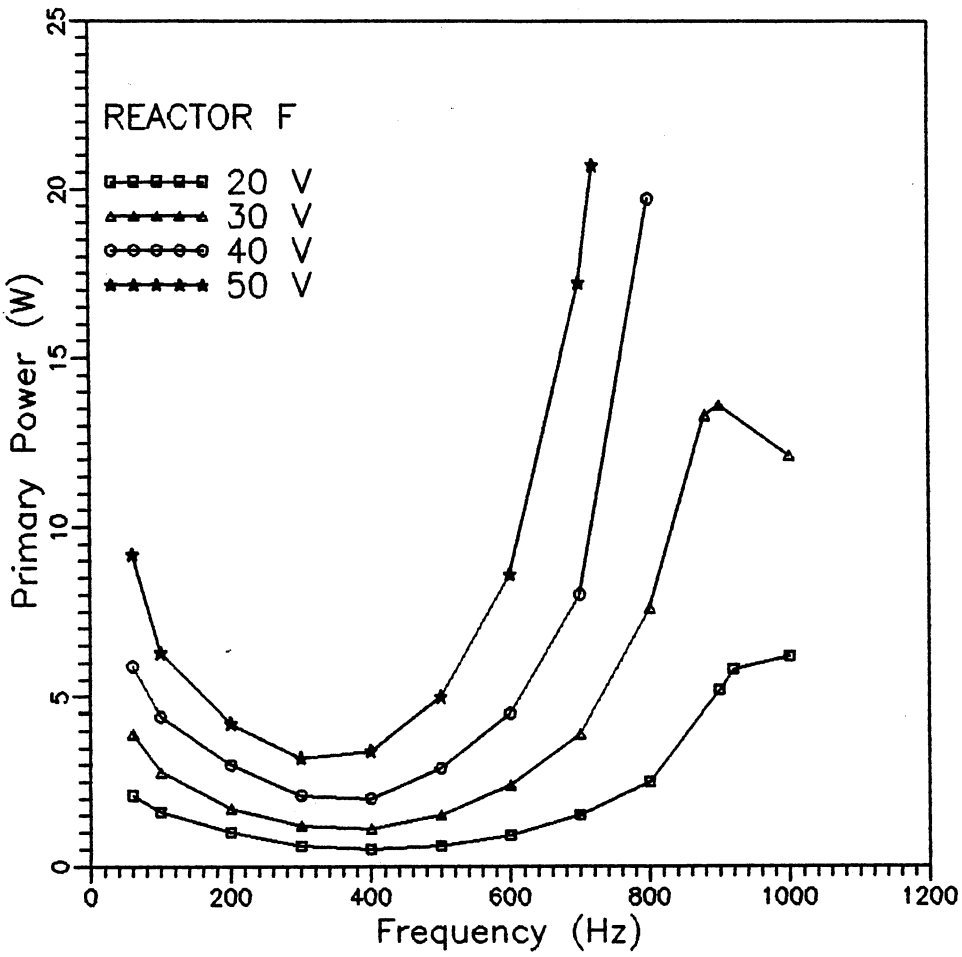

Figure 26. Effect of Frequency and Primary Voltage on Primary Power for Reactor F.

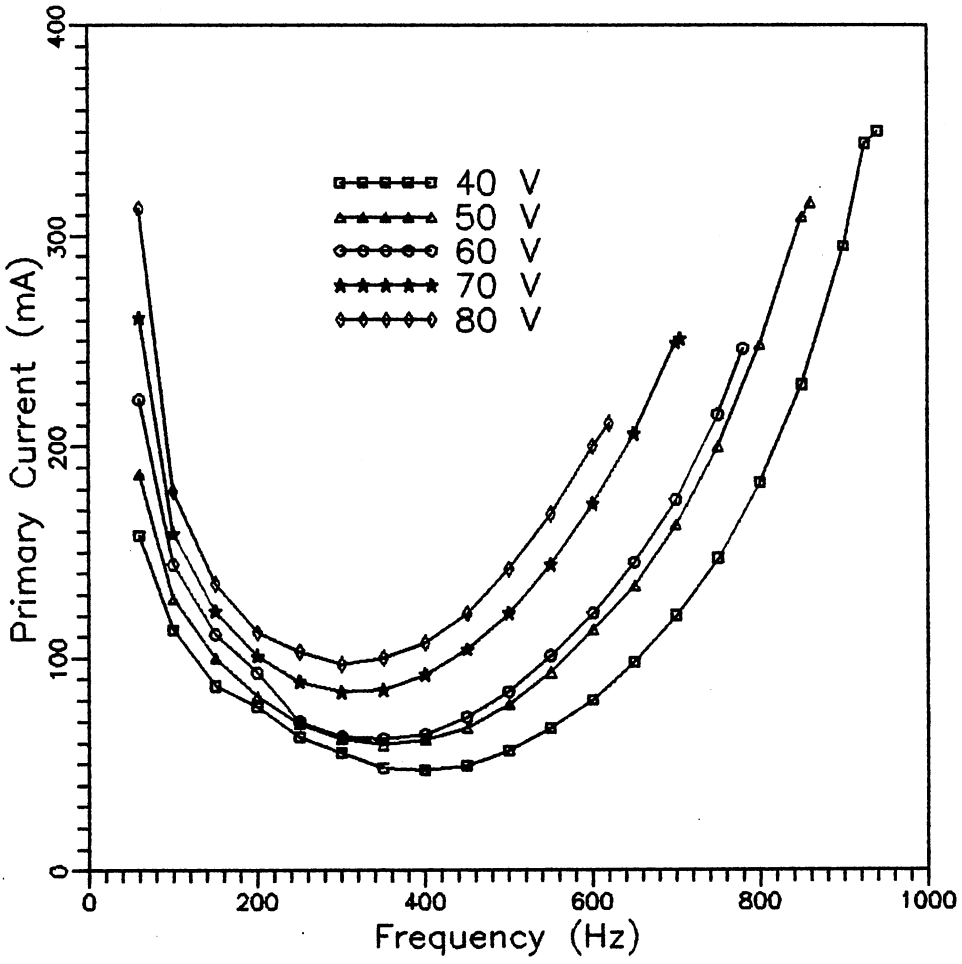

Figure 27. Effect of Frequency on Open-Circuit Primary Current for Various Primary Voltages.

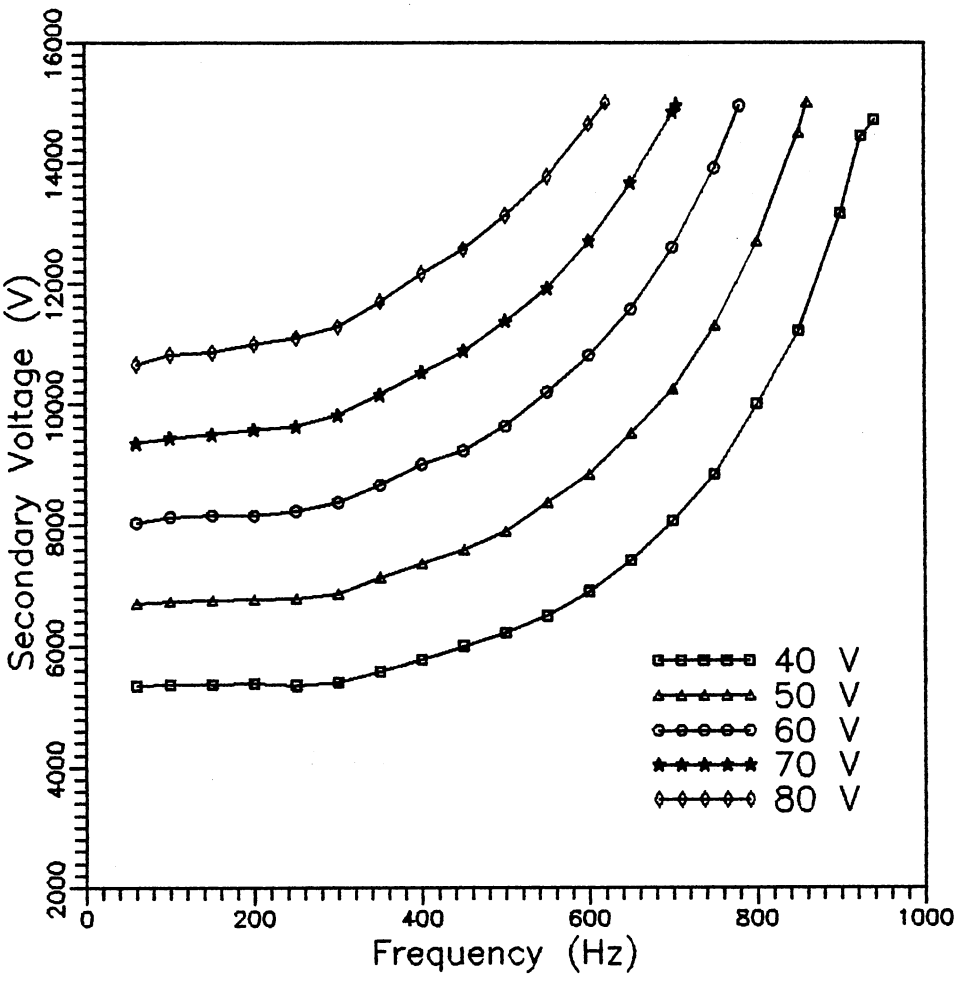

Figure 28. Effect of Frequency on Open-Circuit Secondary Voltage for Various Primary Voltages.

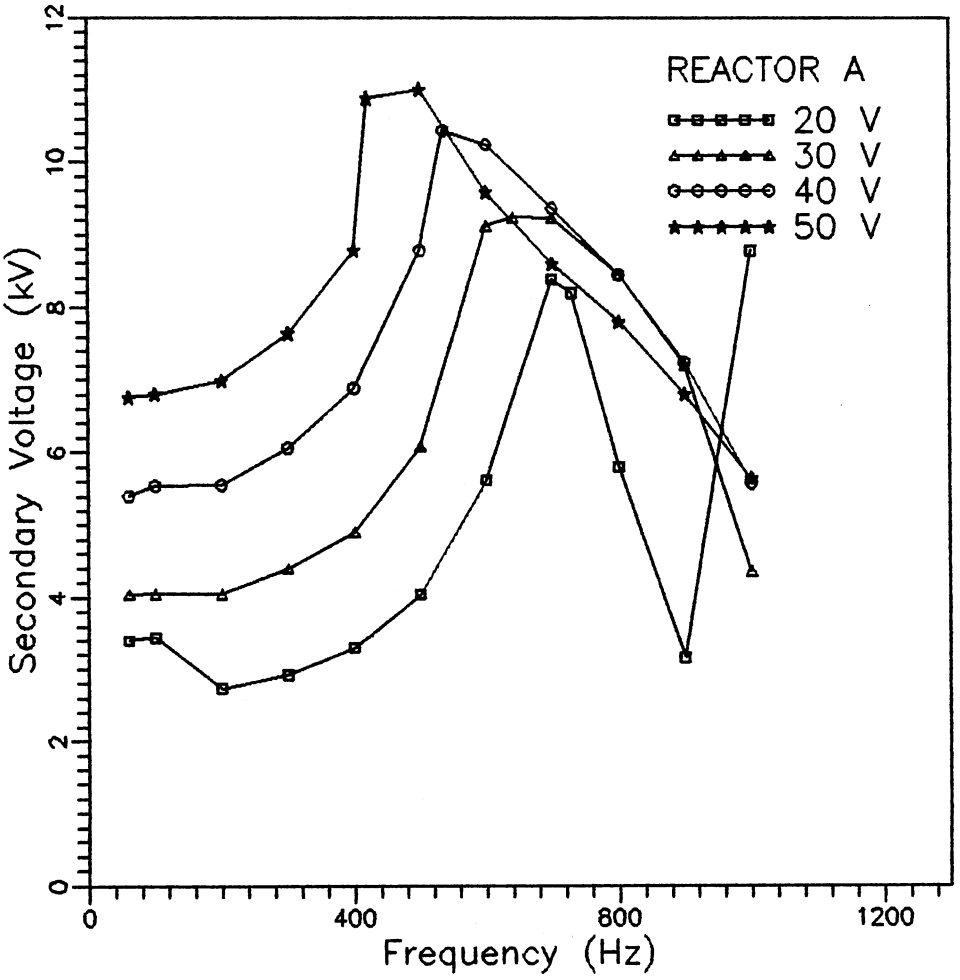

Figure 29. Variation of Secondary Voltage with Frequency and Primary Voltage for Reactor A.

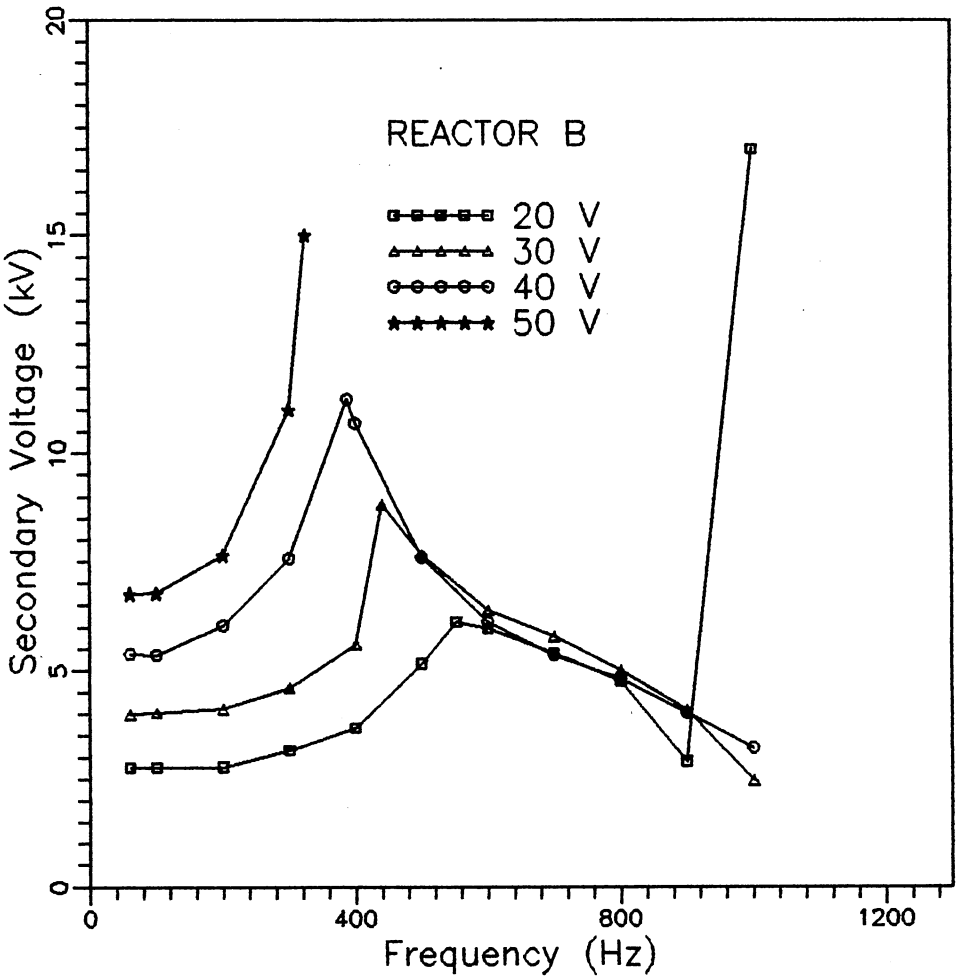

Figure 30. Variation of Secondary Voltage with Frequency and Primary Voltage for Reactor B.

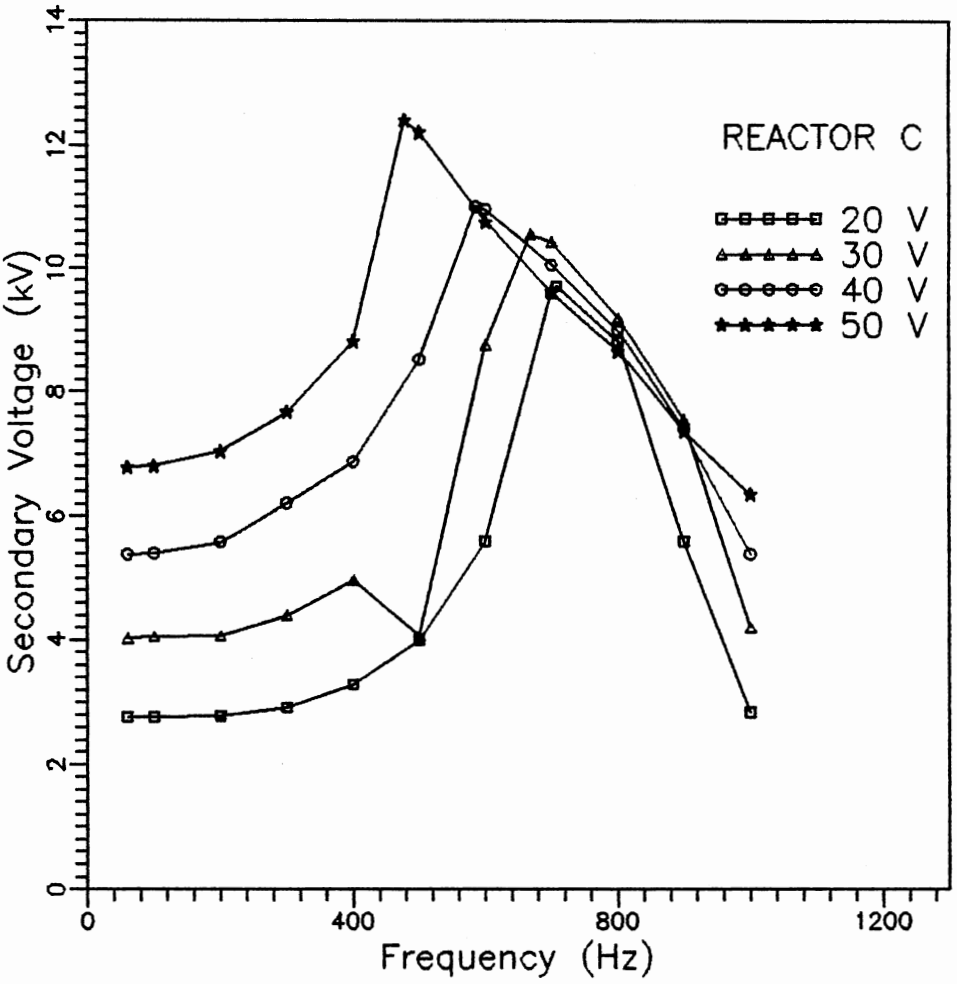

Figure 31. Variation of Secondary Voltage with Frequency and Primary Voltage for Reactor C.

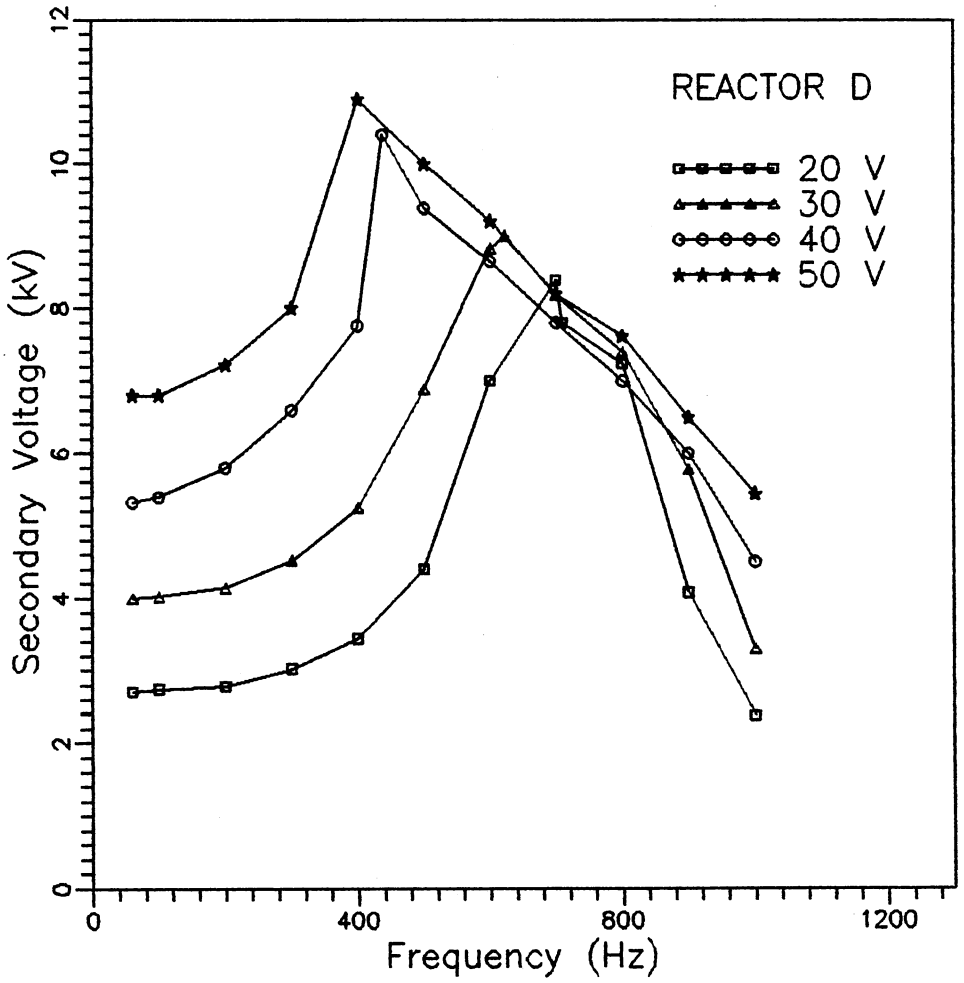

Figure 32. Variation of Secondary Voltage with Frequency and Primary Voltage for Reactor D.

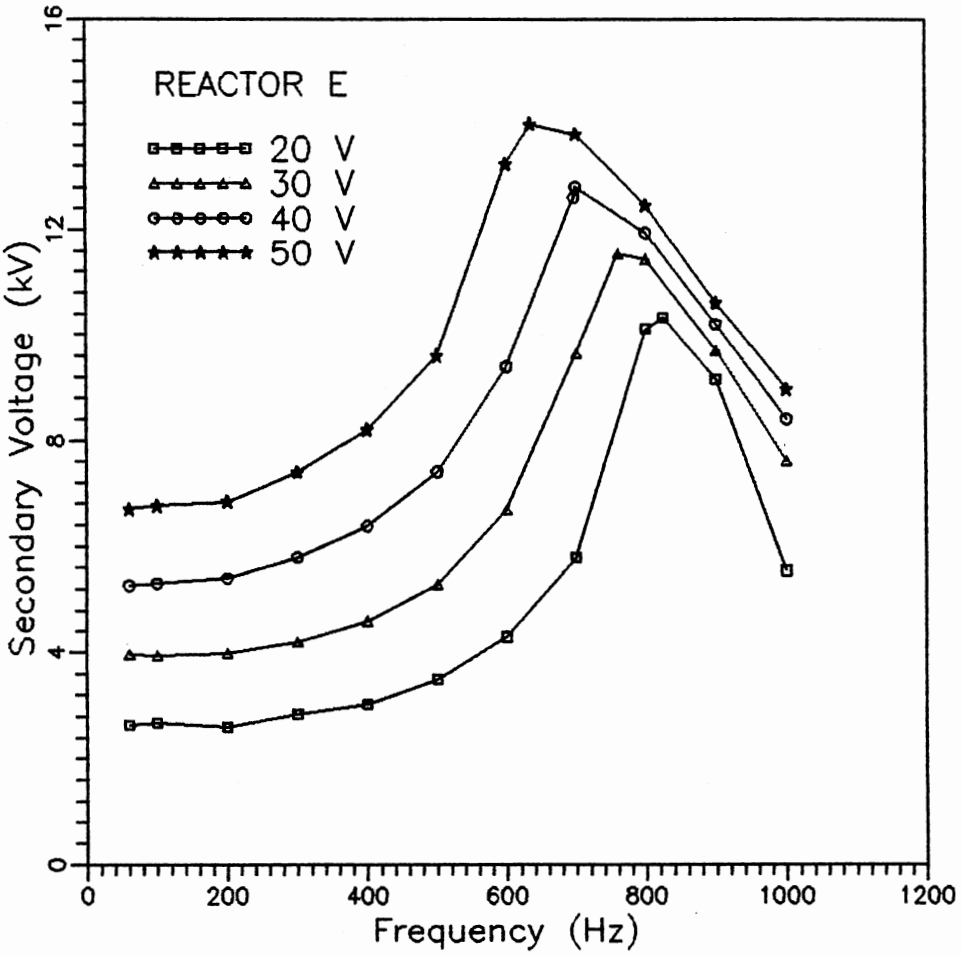

Figure 33. Variation of Secondary Voltage with Frequency and Primary Voltage for Reactor E.

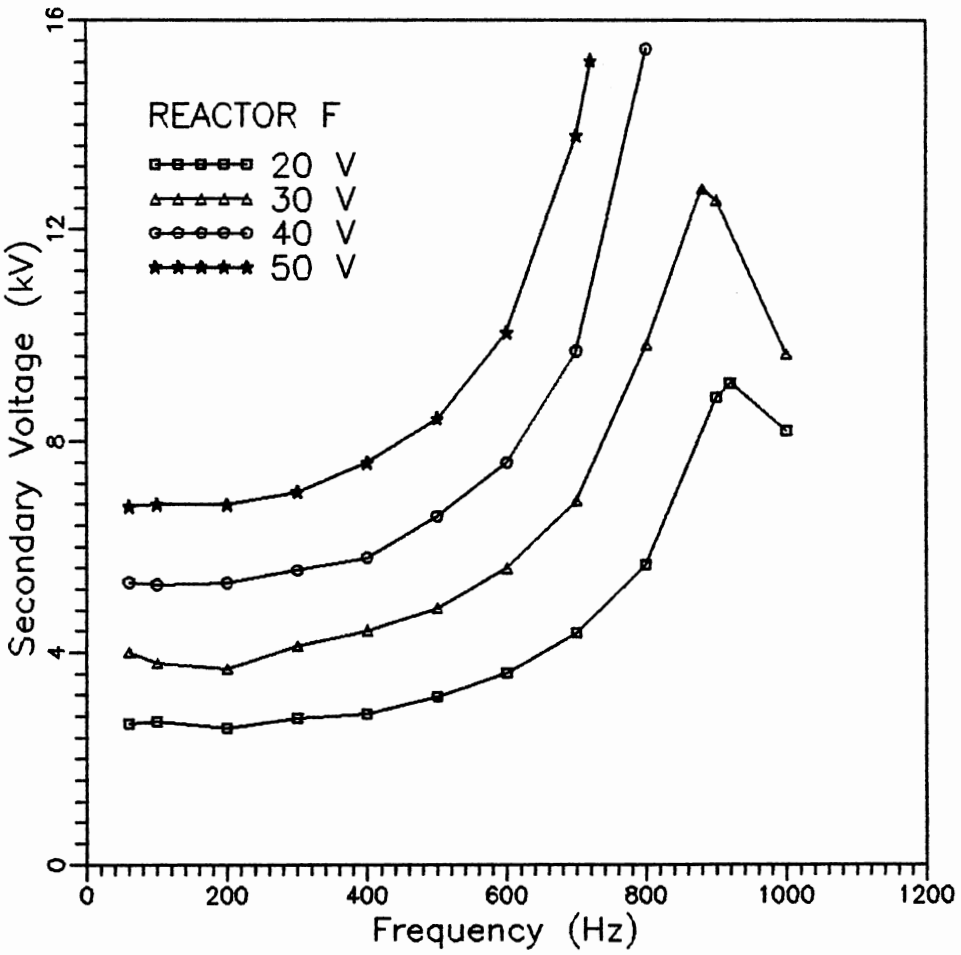

Figure 34. Variation of Secondary Voltage with Frequency and Primary Voltage for Reactor F.

APPENDIX C

OPEN-CIRCUIT TEST DATA

TABLE XII

OPEN-CIRCUIT TEST DATA

V_p (V)	f (Hz)	I_p (mA)	V_s (V)	W_p (W)
40	60	158	5350	6.3
	100	113	5370	4.5
	150	87	5374	3.5
	200	77	5390	3.1
	250	63	5360	2.5
	300	55	5400	2.2
	350	48	5580	1.9
	400	47	5780	1.9
	450	49	6000	1.9
	500	56	6220	2.2
	550	67	6500	2.7
	600	80	6900	3.2
	650	98	7420	3.9
	700	120	8080	4.8
	750	147	8840	5.9
	800	183	10000	7.3
	850	229	11220	9.1
	900	295	13160	11.8
	925	344	14440	13.8
	940	350	14700	14.0
50	60	187	6700	9.3
	100	128	6740	6.4
	150	100	6760	5.0
	200	82	6770	4.1
	250	69	6790	3.5
	300	62	6860	3.1
	350	59	7140	2.9
	400	61	7360	3.0
	450	67	7600	3.4
	500	78	7900	3.9
	550	93	8380	4.7
	600	113	8840	5.6
	650	134	9520	6.7
	700	163	10260	8.1
	750	200	11300	10.0
	800	248	12700	12.4
	850	309	14500	15.5
	860	316	15000	15.8

TABLE XII (continued)

OPEN-CIRCUIT TEST DATA

V_p (V)	f (Hz)	I_p (mA)	V_s (V)	W_p (W)
60	60	222	8040	13.3
	100	144	8140	8.6
	150	111	8160	6.7
	200	93	8160	5.6
	250	70	8240	4.2
	300	63	8380	3.8
	350	62	8660	3.7
	400	64	9000	3.9
	450	72	9240	4.3
	500	84	9640	5.0
	550	101	10200	6.0
	600	121	10810	7.2
	650	145	11580	8.7
	700	175	12600	10.5
	750	215	13900	12.9
	780	246	14940	14.8
70	60	261	9360	18.2
	100	159	9440	11.1
	150	122	9500	8.5
	200	101	9580	7.1
	250	89	9640	6.3
	300	84	9820	5.9
	350	85	10160	6.0
	400	92	10520	6.4
	450	104	10880	7.2
	500	121	11380	8.5
	550	144	11920	10.1
	600	173	12700	12.1
	650	206	13660	14.4
	700	249	14840	17.4
	705	251	14960	17.6
80	60	313	10660	25.1
	100	179	10820	14.3
	150	135	10860	10.8
	200	112	11000	9.0
	250	103	11100	8.2
	300	97	11280	7.8
	350	100	11700	8.0
	400	107	12160	8.5
	450	121	12560	9.7
	500	142	13120	11.3
	550	168	13760	13.5
	600	200	14640	16.0
	620	211	15000	16.9

APPENDIX D

A NOTE ON CORONA DISCHARGE

A Note on Corona Discharge:

Corona is purely a gas-phase phenomenon and it produces free radicals only in a gas or a mixture of gases. In addition to reacting in the gas phase, however, the radicals can interact with molecules of a liquid or of a finely divided solid that is subsequently exposed to them.

Corona starts with a few stray electrons that are always present in a gas because of cosmic rays or other background radiation. When a high voltage, 10000 to 15000 volts, is applied, creating a strong electric field, the electrons are accelerated toward the positive electrode. They strike gas molecules in their path, from which they rebound with little loss of energy because of the great disparity in mass (like a ping-pong ball rebounding from a bowling ball). Then they accelerate again.

Occasionally, by chance, a long enough path opens up for an electron so that when it finally hits the gas molecule, it has acquired enough energy the molecule's shield of orbiting electrons. At this one of the two things can happen. The impacting electron may knock an orbital electron out of the molecule, leaving a positive ion and another free electron that can go on to strike another molecule. More often the impacting electron lifts an orbiting electron to an unstable higher energy orbit, creating an "excited molecule". Soon the gas is full of

electrons, positive ions, excited molecules, heat and light - in other words corona. The excited molecules are unstable; they decompose spontaneously into free radicals. The whole process of corona buildup takes only about a fraction of a second, and it is repeated every time the electric field reverses (Coffman, 1965).

VITA 2

Tarique M. Mangrio

Candidate for the Degree of

Master of Science

Thesis: PRODUCTION OF TITANIUM DIOXIDE POWDER BY THE OXIDATION OF TITANIUM TETRACHLORIDE IN A PLASMA REACTOR

Major Field: Chemical Engineering

Biographical:

Personal Data: Born in Hyderabad, Sind, Pakistan, September 20, 1964, the son of Abdul Razzaq Mangrio and Nighat Mangrio.

Education: Graduated from F.G. Boys High School, Hyderabad, Pakistan, in 1979; received Bachelor of Engineering Degree in Chemical Engineering from Mehran University of Engineering and Technology, Jamshoro, Pakistan, in May 1988; completed requirements for the Master of Science Degree at Oklahoma State University in May 1992.

Professional Experience: Trainee Engineer, Pakistan Oil Refinery Ltd., Karachi, Pakistan, 1988. Research Engineer, Hydrocarbon Development Institute of Pakistan, Karachi, Pakistan, 1989. Graduate Teaching Assistant, School of Chemical Engineering, Oklahoma State University, Stillwater, Oklahoma, 1990-91.